

A Two-Singlet Model for Light Cold Dark Matter

Abdessamad Abada,^{1,*} Salah Nasri,^{2,†} and Djamel Ghaffor^{3,‡}

¹*Laboratoire de Physique des Particules et Physique Statistique,
Ecole Normale Supérieure, BP 92 Vieux Kouba, 16050 Alger, Algeria.*[§]

²*Physics Department, UAE University , Al Ain, United Arab Emirates.*

³*Laboratoire de Physique theorique d'oran -ES-SENIA University , 31000 Oran Algeria.*

(Dated: November 21, 2018)

Abstract

We extend the Standard Model by adding two gauge-singlet \mathbb{Z}_2 -symmetric scalar fields that interact with visible matter only through the Higgs particle. One is a stable dark matter WIMP, and the other one undergoes a spontaneous breaking of the symmetry that opens new channels for the dark matter annihilation, hence lowering the mass of the WIMP. We study the effects of the observed dark matter relic abundance on the annihilation cross section and find that in most regions of the parameters space, light dark matter is viable. We also compare the elastic scattering cross-section of our dark matter candidate off nucleus with existing (CDMSII and XENON100) and projected (SuperCDMS and XENON1T) experimental exclusion bounds. We find that most of the allowed mass range for light dark matter will be probed by the projected sensitivity of XENON1T experiment.

PACS numbers: 95.35.+d; 98.80.-k; 12.15.-y; 11.30.Qc.

Keywords: cold dark matter. light WIMP. extension of Standard Model.

*Electronic address: a.abada@uaeu.ac.ae

†Electronic address: snasri@uaeu.ac.ae

‡Electronic address: dghaffor@mail-enset.dz

§Present address: Physics Department, UAE University, POB 17551, Al Ain, UAE .

I. INTRODUCTION

Cosmology tells us that about 25% of the total mass density in the Universe is dark matter that cannot be accounted for by conventional baryons [1]. Alongside observation, intense theoretical efforts are made in order to elucidate the nature and properties of this unknown form of matter. In this context, electrically neutral and colorless weakly interacting massive particles (WIMPs) form an attractive scenario. Their broad properties are: masses in the range of one to a few hundred GeV, coupling constants in the milli-weak scale and lifetimes longer than the age of the Universe.

Recent data from the direct-detection experiments DAMA/LIBRA [2] and CoGeNT [3], and the recent analysis of the data from the Fermi Gamma Ray Space Telescope [4], if interpreted as signal for dark matter, require light WIMPs in the range of 5 to 10 GeV [5]. Also, galactic substructure requires still lighter dark matter masses [6, 7]. In this regard, it is useful to note in passing that the XENON100 collaboration has provided serious constraints on the region of interest to DAMA/LIBRA and CoGeNT [8], assuming a constant extrapolation of the liquid xenon scintillation response for nuclear recoils below 5 keV, a claim disputed in [9]. Most recently, the CDMS collaboration has released the analysis of their low-energy threshold data [10] which seems to exclude the parameter space for dark matter interpretation of DAMA/LIBRA and CoGeNT results, assuming a standard halo dark matter model with an escape velocity $v_{esc} = 544$ km/s and neglecting the effect of ion channeling [11]. However, with a highly anisotropic velocity distribution, it may be possible to reconcile the CoGeNT and DAMA/LIBRA results with the current exclusion limits from CDMS and XENON [12] (see also comments on p.6 in [13] about the possibility of shifting the exclusion contour in [10] above the CoGeNT signal region). In addition, CRESST, another direct detection experiment at Gran Sasso, which uses CaWO_4 as target material, reported in talks at the IDM 2010 and WONDER 2010 workshops an excess of events in their oxygen band instead of tungsten band. If this signal is not due to neutron background a possible interpretation could be the elastic scattering of a light WIMP depositing a detectable recoil energy on the the lightest nuclei (oxygen) in the detector [14]. While this result has to await confirmation from the CRESST collaboration, it is clear that it is important as well as interesting to study light dark matter.

The most popular candidate for dark matter is the neutralino, a neutral R -odd supersymmetric particle. Indeed, they are only produced or destroyed in pairs, thus rendering the lightest SUSY particle (LSP) stable [15]. In the minimal version of the supersymmetric extension of the Standard Model, the neutralino is a linear combination of the fermionic partners of the neutral electroweak gauge bosons (gauginos) and the neutral Higgs bosons (higgsinos). They can annihilate through a t-channel sfermion exchange into standard model fermions, or via a t-channel chargino-mediated process into W^+W^- , or through an s-channel pseudoscalar Higgs exchange into fermion pairs and they can undergo elastic scattering with nuclei mainly through scalar Higgs exchange [16]. If these

neutralinos were light, they would then be overproduced in the early universe and, in the minimal model, would not have an elastic-scattering cross section large enough to account for the DAMA/LIBRA and CoGeNT results due to constraints from other experiments such as the LEP, Tevatron, and rare decays [17–19].

Therefore, with no clear clue yet as to what the internal structure of these WIMPs is, if any, a pedestrian approach can be attractive. In this logic, the simplest of models is to extend the Standard Model by adding a real scalar field, the dark matter, a Standard-Model gauge singlet that interacts with visible particles via the Higgs field only. To ensure stability, it is endowed with a discrete \mathbb{Z}_2 symmetry that does not spontaneously break. Such a model can be seen as a low-energy remnant of some higher-energy physics waiting to be understood. In this cosmological setting, such an extension has first been proposed in [20] and further studied in [21] where the unbroken \mathbb{Z}_2 symmetry is extended to a global U(1) symmetry. A more extensive exploration of the model and its implications was done in [22], specific implications on Higgs detection and LHC physics discussed in [23] and one-loop vacuum stability looked into and perturbativity bounds obtained in [24]. The work of [25] considers also this minimal extension and uses constraints from the experiments XENON10 [26] and CDMSII [27] to exclude dark matter masses smaller than 50, 70 and 75GeV for Higgs masses equal to 120, 200 and 350 GeV respectively.

In order to allow for light dark matter, it is therefore necessary to go beyond the minimal one-real-scalar extension of the Standard Model. The natural next step is to add another real scalar field, endowed with a \mathbb{Z}_2 symmetry too, but one which is spontaneously broken so that new channels for dark matter annihilation are opened, increasing this way the annihilation cross-section, hence allowing smaller masses. This auxiliary field must also be a Standard Model gauge singlet.

After this brief introductory motivation, we present the model in the next section. We perform the spontaneous breaking of the electroweak and the additional \mathbb{Z}_2 symmetries in the usual way. We clarify the physical modes as well as the physical parameters. There is mixing between the physical new scalar field and the Higgs, and this is one of the quantities parametrizing the subsequent physics. In section three, we impose the constraint from the known dark matter relic density on the dark-matter annihilation cross section and study its effects. Of course, as we will see, the parameter space is quite large, and so, it is not realistic to hope to cover all of it in one single work of acceptable size. Representative values have to be selected and the behavior of the model as well as its capabilities are described. Our main focus in this study is the mass range 0.1GeV – 100GeV and we find that the model is rich enough to bear dark matter in most of it, including the very light sector. In section four, we determine the total cross section σ_{det} for non relativistic elastic scattering of dark matter off a nucleon target and compare it to the current direct-detection experimental bounds and projected sensitivity. For this, we choose the results of CDMSII and XENON100, and the projections of SuperCDMS [28] and XENON1T [29]. Here too we cannot cover all of the parameter space nor are we going to give a detailed account of the behavior of σ_{det} as a function of the dark matter

mass, but general patterns are mentioned. The last section is devoted to some concluding remarks. Note that as a rule, we have avoided in this first study narrowing the choice of parameters using particle phenomenology. Of course, such phenomenological constraints have to be addressed ultimately and this is left to a forthcoming investigation, contenting ourselves in the present work with a limited set of remarks mentioned in this last section. Finally, we have gathered in an appendix the partial results regarding the calculation of the dark matter annihilation cross section.

II. A TWO-SINGLET MODEL FOR DARK MATTER

We extend the Standard Model by adding two real, spinless and \mathbb{Z}_2 -symmetric fields: the dark matter field S_0 for which the \mathbb{Z}_2 symmetry is unbroken and an auxiliary field χ_1 for which it is spontaneously broken. Both fields are Standard Model gauge singlets and hence can interact with ‘visible’ particles only via the Higgs doublet H . This latter is taken in the unitary gauge such that $H^\dagger = 1/\sqrt{2}(0 \ h')$, where h' is a real scalar. We assume all processes calculable in perturbation theory. The potential function that includes S_0 , h' and χ_1 writes as follows:

$$U = \frac{\tilde{m}_0^2}{2} S_0^2 - \frac{\mu^2}{2} h'^2 - \frac{\mu_1^2}{2} \chi_1^2 + \frac{\eta_0}{24} S_0^4 + \frac{\lambda}{24} h'^4 + \frac{\eta_1}{24} \chi_1^4 + \frac{\lambda_0}{4} S_0^2 h'^2 + \frac{\eta_{01}}{4} S_0^2 \chi_1^2 + \frac{\lambda_1}{4} h'^2 \chi_1^2, \quad (2.1)$$

where \tilde{m}_0^2 , μ^2 and μ_1^2 and all the coupling constants are real positive numbers. In the Standard Model scenario, electroweak spontaneous symmetry breaking occurs for the Higgs field, which then oscillates around the vacuum expectation value $v = 246\text{GeV}$ [30]. The field χ_1 will oscillate around the vacuum expectation value $v_1 > 0$. Both v and v_1 are related to the parameters of the theory by the two relations:

$$v^2 = 6 \frac{\mu^2 \eta_1 - 6 \mu_1^2 \lambda_1}{\lambda \eta_1 - 36 \lambda_1^2}; \quad v_1^2 = 6 \frac{\mu_1^2 \lambda - 6 \mu^2 \lambda_1}{\lambda \eta_1 - 36 \lambda_1^2}. \quad (2.2)$$

It is assumed that the self-coupling constants are sufficiently larger than the mutual ones.

Writing $h' = v + \tilde{h}$ and $\chi_1 = v_1 + \tilde{S}_1$, the potential function becomes, up to an irrelevant zero-field energy:

$$U = U_{\text{quad}} + U_{\text{cub}} + U_{\text{quar}}, \quad (2.3)$$

where the mass-squared (quadratic) terms are gathered in U_{quad} , the cubic interactions in U_{cub} and the quartic ones in U_{quar} . The quadratic terms are given by:

$$U_{\text{quad}} = \frac{1}{2} m_0^2 S_0^2 + \frac{1}{2} M_h^2 \tilde{h}^2 + \frac{1}{2} M_1^2 \tilde{S}_1^2 + M_{1h}^2 \tilde{h} \tilde{S}_1, \quad (2.4)$$

where the mass-squared coefficients are related to the original parameters of the theory by the following relations:

$$\begin{aligned} m_0^2 &= \tilde{m}_0^2 + \frac{\lambda_0}{2} v^2 + \frac{\eta_{01}}{2} v_1^2; & M_h^2 &= -\mu^2 + \frac{\lambda}{2} v^2 + \frac{\lambda_1}{2} v_1^2; \\ M_1^2 &= -\mu_1^2 + \frac{\lambda_1}{2} v^2 + \frac{\eta_1}{2} v_1^2; & M_{1h}^2 &= \lambda_1 v v_1. \end{aligned} \quad (2.5)$$

Replacing the vacuum expectation values v and v_1 by their respective expressions (2.2) will not add clarity. In this field basis, the mass-squared matrix is not diagonal: there is mixing between the fields \tilde{h} and \tilde{S}_1 . Denoting the physical mass-squared field eigenmodes by h and S_1 , we rewrite:

$$U_{\text{quad}} = \frac{1}{2}m_0^2 S_0^2 + \frac{1}{2}m_h^2 h^2 + \frac{1}{2}m_1^2 S_1^2, \quad (2.6)$$

where the physical fields are related to the mixed ones by a 2×2 rotation:

$$\begin{pmatrix} h \\ S_1 \end{pmatrix} = \begin{pmatrix} \cos \theta & \sin \theta \\ -\sin \theta & \cos \theta \end{pmatrix} \begin{pmatrix} \tilde{h} \\ \tilde{S}_1 \end{pmatrix}. \quad (2.7)$$

Here θ is the mixing angle, related to the original mass-squared parameters by the relation:

$$\tan 2\theta = \frac{2M_{1h}^2}{M_1^2 - M_h^2}, \quad (2.8)$$

and the physical masses in (2.6) by the two relations:

$$\begin{aligned} m_h^2 &= \frac{1}{2} \left[M_h^2 + M_1^2 + \varepsilon (M_h^2 - M_1^2) \sqrt{(M_h^2 - M_1^2)^2 + 4M_{1h}^4} \right]; \\ m_1^2 &= \frac{1}{2} \left[M_h^2 + M_1^2 - \varepsilon (M_h^2 - M_1^2) \sqrt{(M_h^2 - M_1^2)^2 + 4M_{1h}^4} \right], \end{aligned} \quad (2.9)$$

where ε is the sign function.

Written now directly in terms of the physical fields, the cubic interaction terms are expressed as follows:

$$U_{\text{cub}} = \frac{\lambda_0^{(3)}}{2} S_0^2 h + \frac{\eta_{01}^{(3)}}{2} S_0^2 S_1 + \frac{\lambda^{(3)}}{6} h^3 + \frac{\eta_1^{(3)}}{6} S_1^3 + \frac{\lambda_1^{(3)}}{2} h^2 S_1 + \frac{\lambda_2^{(3)}}{2} h S_1^2, \quad (2.10)$$

where the cubic physical coupling constants are related to the original parameters via the following relations:

$$\begin{aligned} \lambda_0^{(3)} &= \lambda_0 v \cos \theta + \eta_{01} v_1 \sin \theta; \\ \eta_{01}^{(3)} &= \eta_{01} v_1 \cos \theta - \lambda_0 v \sin \theta; \\ \lambda^{(3)} &= \lambda v \cos^3 \theta + \frac{3}{2} \lambda_1 \sin 2\theta (v_1 \cos \theta + v \sin \theta) + \eta_1 v_1 \sin^3 \theta; \\ \eta_1^{(3)} &= \eta_1 v_1 \cos^3 \theta - \frac{3}{2} \lambda_1 \sin 2\theta (v \cos \theta - v_1 \sin \theta) - \lambda v \sin^3 \theta; \\ \lambda_1^{(3)} &= \lambda_1 v_1 \cos^3 \theta + \frac{1}{2} \sin 2\theta [(2\lambda_1 - \lambda) v \cos \theta - (2\lambda_1 - \eta_1) v_1 \sin \theta] - \lambda_1 v \sin^3 \theta; \\ \lambda_2^{(3)} &= \lambda_1 v \cos^3 \theta - \frac{1}{2} \sin 2\theta [(2\lambda_1 - \eta_1) v_1 \cos \theta + (2\lambda_1 - \lambda) v \sin \theta] + \lambda_1 v_1 \sin^3 \theta. \end{aligned} \quad (2.11)$$

Also, in terms of the physical fields, the quartic interactions are given by:

$$\begin{aligned}
U_{\text{quar}} = & \frac{\eta_0}{24} S_0^4 + \frac{\lambda^{(4)}}{24} h^4 + \frac{\eta_1^{(4)}}{24} S_1^4 + \frac{\lambda_0^{(4)}}{4} S_0^2 h^2 + \frac{\eta_{01}^{(4)}}{4} S_0^2 S_1^2 + \frac{\lambda_{01}^{(4)}}{2} S_0^2 h S_1 \\
& + \frac{\lambda_1^{(4)}}{6} h^3 S_1 + \frac{\lambda_2^{(4)}}{4} h^2 S_1^2 + \frac{\lambda_3^{(4)}}{6} h S_1^3,
\end{aligned} \tag{2.12}$$

where the physical quartic coupling constants are written in terms of the original parameters of the theory as follows:

$$\begin{aligned}
\lambda^{(4)} &= \lambda \cos^4 \theta + \frac{3}{2} \lambda_1 \sin^2 2\theta + \eta_1 \sin^4 \theta; \\
\eta_1^{(4)} &= \eta_1 \cos^4 \theta + \frac{3}{2} \lambda_1 \sin^2 2\theta + \lambda \sin^4 \theta; \\
\lambda_0^{(4)} &= \lambda_0 \cos^2 \theta + \eta_{01} \sin^2 \theta; \\
\eta_{01}^{(4)} &= \eta_{01} \cos^2 \theta + \lambda_0 \sin^2 \theta; \\
\lambda_{01}^{(4)} &= \frac{1}{2} (\eta_{01} - \lambda_0) \sin 2\theta; \\
\lambda_1^{(4)} &= \frac{1}{2} [(3\lambda_1 - \lambda) \cos^2 \theta - (3\lambda_1 - \eta_1) \sin^2 \theta] \sin 2\theta; \\
\lambda_2^{(4)} &= \lambda_1 \cos^2 2\theta - \frac{1}{4} (2\lambda_1 - \eta_1 - \lambda) \sin^2 2\theta; \\
\lambda_3^{(4)} &= \frac{1}{2} [(\eta_1 - 3\lambda_1) \cos^2 \theta - (\lambda - 3\lambda_1) \sin^2 \theta] \sin 2\theta.
\end{aligned} \tag{2.13}$$

Finally, after spontaneous breaking of the electroweak and \mathbb{Z}_2 symmetries, the part of the Standard Model lagrangian that is relevant to dark matter annihilation writes, in terms of the physical fields h and S_1 , as follows:

$$\begin{aligned}
U_{\text{SM}} = & \sum_f (\lambda_{hf} h \bar{f} f + \lambda_{1f} S_1 \bar{f} f) + \lambda_{hw}^{(3)} h W_\mu^- W^{+\mu} + \lambda_{1w}^{(3)} S_1 W_\mu^- W^{+\mu} \\
& + \lambda_{hz}^{(3)} h (Z_\mu)^2 + \lambda_{1z}^{(3)} S_1 (Z_\mu)^2 + \lambda_{hw}^{(4)} h^2 W_\mu^- W^{+\mu} + \lambda_{1w}^{(4)} S_1^2 W_\mu^- W^{+\mu} \\
& + \lambda_{h1w} h S_1 W_\mu^- W^{+\mu} + \lambda_{hz}^{(4)} h^2 (Z_\mu)^2 + \lambda_{1z}^{(4)} S_1^2 (Z_\mu)^2 + \lambda_{h1z} h S_1 (Z_\mu)^2.
\end{aligned} \tag{2.14}$$

The quantities m_f , m_w and m_z are the masses of the fermion f , the W and the Z gauge bosons respectively, and the above coupling constants are given by the following relations:

$$\begin{aligned}
\lambda_{hf} &= -\frac{m_f}{v} \cos \theta; & \lambda_{1f} &= \frac{m_f}{v} \sin \theta; \\
\lambda_{hw}^{(3)} &= 2\frac{m_w^2}{v} \cos \theta; & \lambda_{1w}^{(3)} &= -2\frac{m_w^2}{v} \sin \theta; \\
\lambda_{hz}^{(3)} &= \frac{m_z^2}{v} \cos \theta; & \lambda_{1z}^{(3)} &= -\frac{m_z^2}{v} \sin \theta; \\
\lambda_{hw}^{(4)} &= \frac{m_w^2}{v^2} \cos^2 \theta; & \lambda_{1w}^{(4)} &= \frac{m_w^2}{v^2} \sin^2 \theta; & \lambda_{h1w} &= -\frac{m_w^2}{v^2} \sin 2\theta; \\
\lambda_{hz}^{(4)} &= \frac{m_z^2}{2v^2} \cos^2 \theta; & \lambda_{1z}^{(4)} &= \frac{m_z^2}{2v^2} \sin^2 \theta; & \lambda_{h1z} &= -\frac{m_z^2}{2v^2} \sin 2\theta.
\end{aligned} \tag{2.15}$$

III. RELIC DENSITY, MUTUAL COUPLINGS AND PERTURBATIVITY

The original theory (2.1) has nine parameters: three mass parameters (\tilde{m}_0, μ, μ_1), three self-coupling constants (η_0, λ, η_1) and three mutual coupling constants ($\lambda_0, \eta_{01}, \lambda_1$). Perturbativity is assumed, hence all these original coupling constants are small. The dark-matter self-coupling constant η_0 does not enter in the calculations of the lowest-order processes of this work [31], so effectively, we are left with eight parameters. The spontaneous breaking of the electroweak and \mathbb{Z}_2 symmetries for the Higgs and χ_1 fields respectively introduces the two vacuum expectation values v and v_1 given to lowest order in (2.2). The value of v is fixed experimentally to be 246GeV and for the present work, we fix the value of v_1 at the order of the electroweak scale, say 100GeV. Hence we are left with six parameters. Four of these are chosen to be the three physical masses m_0 (dark matter), m_1 (S_1 field) and m_h (Higgs), plus the mixing angle θ between S_1 and h . We will fix the Higgs mass to $m_h = 138\text{GeV}$ and give, in this section, the mixing angle θ the two values 10° (small) and 40° (larger). The two last parameters we choose are the two physical mutual coupling constants $\lambda_0^{(4)}$ (dark matter – Higgs) and $\eta_{01}^{(4)}$ (dark matter – S_1 particle), see (2.12).

In the framework of the thermal dynamics of the Universe within the standard cosmological model [32], the WIMP relic density is related to its annihilation rate by the familiar relations:

$$\begin{aligned}\Omega_D \bar{h}^2 &\simeq \frac{1.07 \times 10^9 x_f}{\sqrt{g_*} m_{\text{Pl}} \langle v_{12} \sigma_{\text{ann}} \rangle \text{GeV}}; \\ x_f &\simeq \ln \frac{0.038 m_{\text{Pl}} m_0 \langle v_{12} \sigma_{\text{ann}} \rangle}{\sqrt{g_*} x_f}.\end{aligned}\tag{3.1}$$

The notation is as follows: the quantity \bar{h} is the Hubble constant in units of 100km/(s×Mpc), $m_{\text{Pl}} = 1.22 \times 10^{19}\text{GeV}$ the Planck mass, m_0 the dark matter mass, $x_f = m_0/T_f$ the ratio of the dark matter mass to the freeze-out temperature T_f and g_* the number of relativistic degrees of freedom with a mass less than T_f . The quantity $\langle v_{12} \sigma_{\text{ann}} \rangle$ is the thermally averaged annihilation cross-section of a pair of two dark matter particles multiplied by their relative speed in the center-of-mass reference frame. Solving (3.1) with the current value for the dark matter relic density $\Omega_D \bar{h}^2 = 0.105 \pm 0.008$ [33] gives:

$$\langle v_{12} \sigma_{\text{ann}} \rangle \simeq (1.9 \pm 0.2) \times 10^{-9} \text{GeV}^{-2},\tag{3.2}$$

for a range of dark matter masses between roughly 10GeV to 100GeV and x_f between 19.2 and 21.6, with about 0.4 thickness [34].

The value in (3.2) for the dark matter annihilation cross-section translates into a relation between the parameters of a given theory entering the calculated expression of $\langle v_{12} \sigma_{\text{ann}} \rangle$, hence imposing a constraint on these parameters which will limit the intervals of possible dark matter masses. This constraint can be exploited to examine aspects of the theory like perturbativity. For example, in our model, we can obtain via (3.2) the

mutual coupling constant $\eta_{01}^{(4)}$ for given values of $\lambda_0^{(4)}$, study its behavior as a function of m_0 and tell which dark-matter mass regions are consistent with perturbativity. Note that once the two mutual coupling constants $\lambda_0^{(4)}$ and $\eta_{01}^{(4)}$ are perturbative, all the other physical coupling constants will be. In the study of this section, we choose the values $\lambda_0^{(4)} = 0.01$ (very weak), 0.2 (weak) and 1 (large). We also let the two masses m_0 and m_1 stretch from 0.1GeV to 120GeV, occasionally m_0 to 200GeV. Finally, note that we do not incorporate the uncertainty in (3.2) when imposing the relic-density constraint, something that is sufficient in view of the descriptive nature of this work.

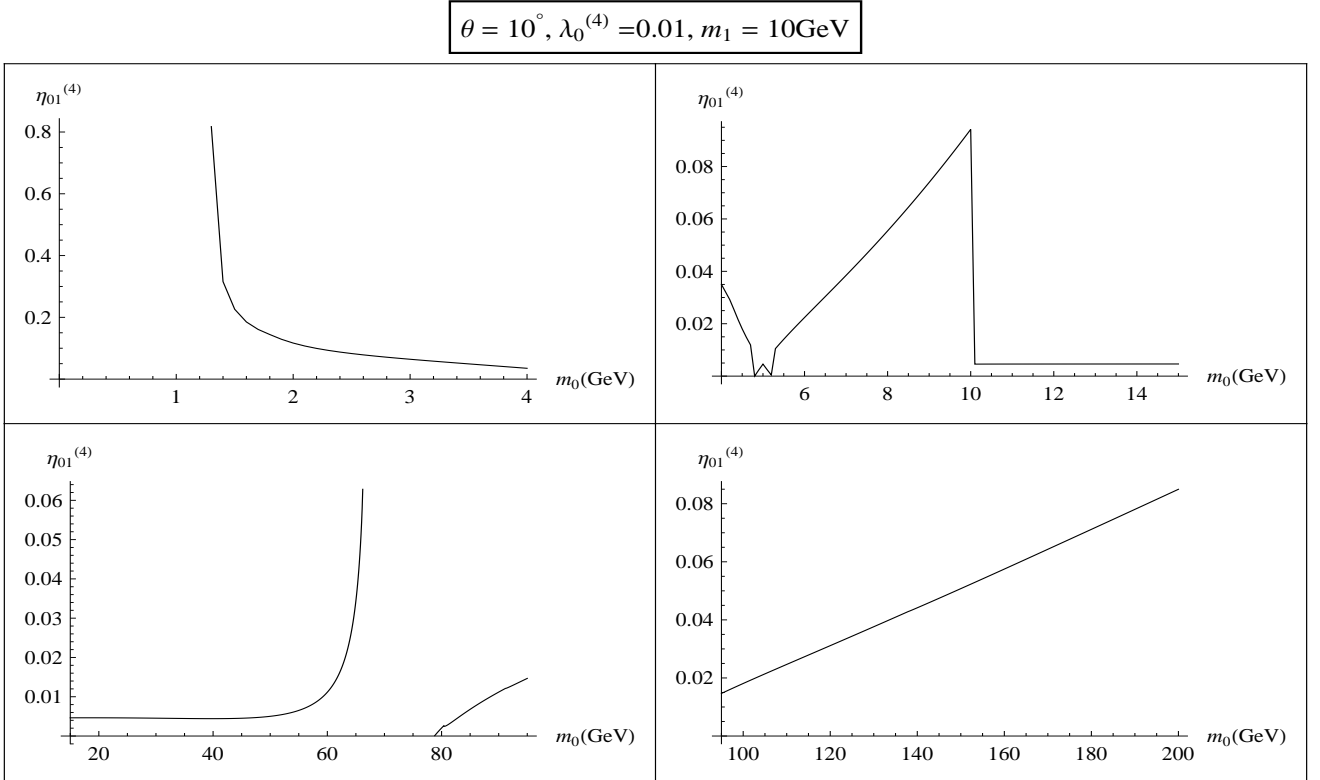


FIG. 1: $\eta_{01}^{(4)}$ vs m_0 for small m_1 , small mixing and very small WIMP-Higgs coupling.

The dark matter annihilation cross sections (times the relative speed) through all possible channels are given in the appendix. The quantity $\langle v_{12}\sigma_{\text{ann}} \rangle$ is the sum of all these contributions. Imposing $\langle v_{12}\sigma_{\text{ann}} \rangle = 1.9 \times 10^{-9} \text{GeV}^{-2}$ dictates the behavior of $\eta_{01}^{(4)}$, which is displayed as a function of the dark matter mass m_0 . Of course, as the parameters are numerous, the behavior is bound to be rich and diverse. We cannot describe every bit of it. Also, one has to note from the outset that for a given set of values for the parameters, the solution to the relic-density constraint is not unique: besides positive real solutions (when they exist), we may find negative real or even complex solutions. It is beyond the scope of the present work to investigate the nature and behavior of all the solutions. We

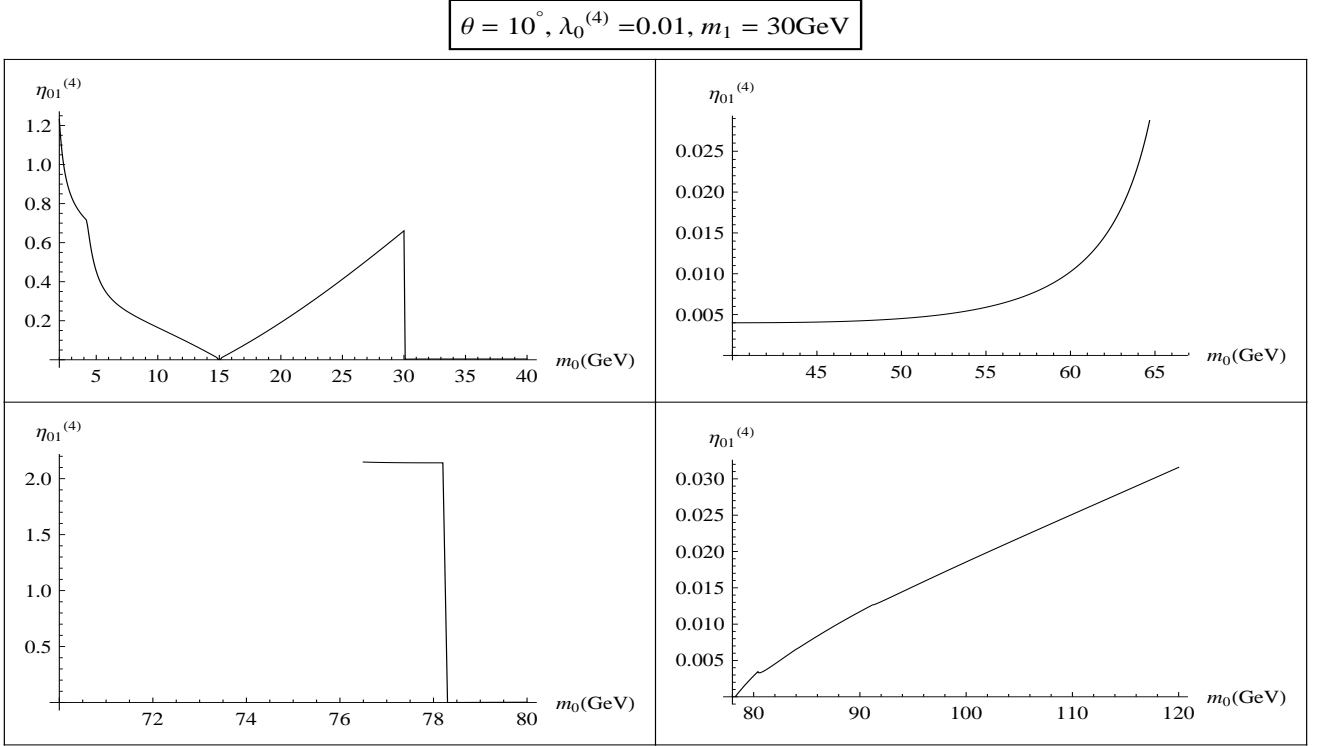


FIG. 2: $\eta_{01}^{(4)}$ vs m_0 for moderate m_1 , small mixing and very small WIMP-Higgs coupling.

are only interested in finding the smallest positive real solution $\eta_{01}^{(4)}$ when it exists, looking at its behavior and finding out when it is small enough to be perturbative.

A. Small mixing angle and very weak dark matter – Higgs coupling

Let us describe briefly and only partly how the mutual $S_0 - S_1$ coupling constant $\eta_{01}^{(4)}$ behaves as a function of the S_0 mass m_0 . We start by a small mixing angle, say $\theta = 10^\circ$, and a very weak mutual $S_0 - \text{Higgs}$ coupling constant, say $\lambda_0^{(4)} = 0.01$. Let us also fix the S_1 mass first at the small value $m_1 = 10\text{GeV}$. The corresponding behavior of $\eta_{01}^{(4)}$ versus m_0 is shown in Fig. 1.

The range of m_0 shown is from 0.1GeV to 200GeV , cut in four intervals to allow for ‘local’ features to be displayed*. We see that the relic-density constraint on S_0 annihilation has no positive real solution for $m_0 \lesssim 1.3\text{GeV}$, and so, with these very small masses, S_0 cannot be a dark matter candidate. In other words, for $m_1 = 10\text{GeV}$, the particle S_0 cannot annihilate into the lightest fermions only; inclusion of the c -quark is necessary. Note that right about $m_0 \simeq 1.3\text{GeV}$, the c threshold, the mutual coupling constant $\eta_{01}^{(4)}$

* A logplot in this descriptive study is not advisable.

$$\theta = 10^\circ, \lambda_0^{(4)} = 0.01, m_0 = 0.2\text{GeV}$$

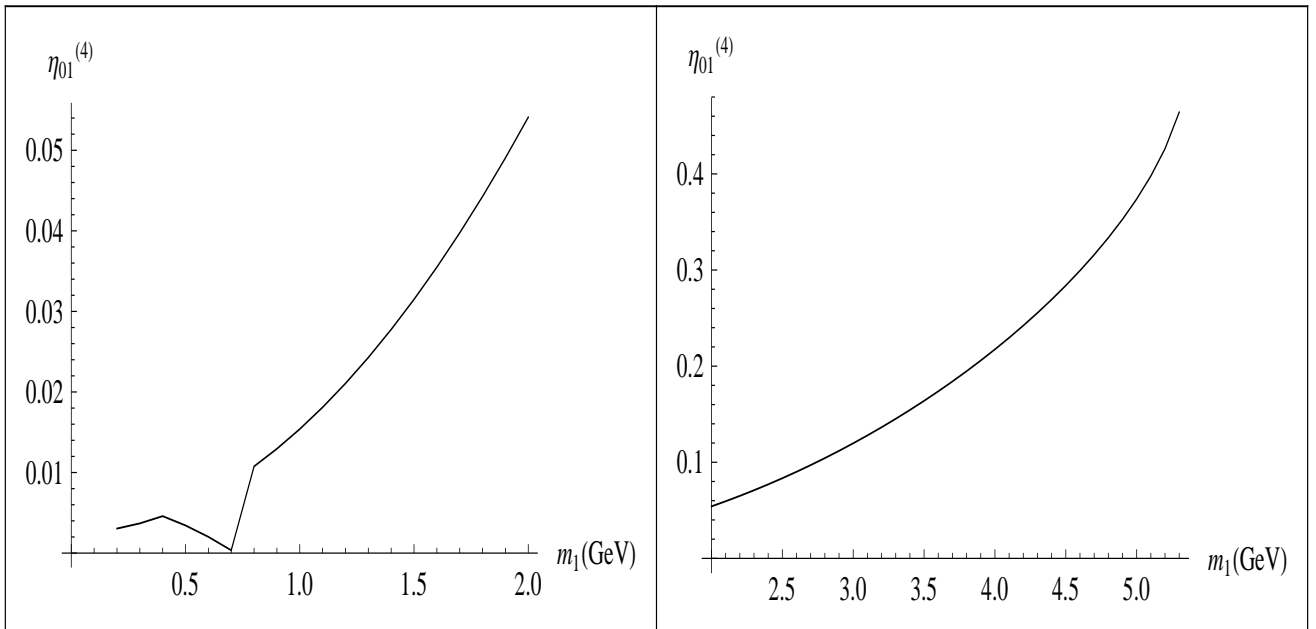


FIG. 3: $\eta_{01}^{(4)}$ vs m_1 for very light S_1 , small mixing and very small WIMP-Higgs coupling.

starts at about 0.8, a value, while perturbative, that is roughly eighty-two-fold larger than the mutual S_0 – Higgs coupling constant $\lambda_0^{(4)}$. Then $\eta_{01}^{(4)}$ decreases, steeply first, more slowly as we cross the τ mass towards the b mass. Just before $m_1/2$, the coupling $\eta_{01}^{(4)}$ hops onto another solution branch that is just emerging from negative territory, gets back to the first one at precisely $m_1/2$ as this latter carries now smaller values, and then jumps up again onto the second branch as the first crosses the m_0 -axis down. It goes up this branch with a moderate slope until m_0 becomes equal to m_1 , a value at which the S_1 annihilation channel opens. Right beyond m_1 , there is a sudden fall to a value $\eta_{01}^{(4)} \simeq 0.0046$ that is about half the value of $\lambda_0^{(4)}$, and $\eta_{01}^{(4)}$ stays flat till $m_0 \simeq 45\text{GeV}$ where it starts increasing, sharply after 60GeV . In the mass interval $m_0 \simeq 66\text{GeV} - 79\text{GeV}$, there is a desert with no positive real solutions to the relic-density constraint, hence no viable dark matter candidate. Beyond $m_0 \simeq 79\text{GeV}$, the mutual coupling constant $\eta_{01}^{(4)}$ keeps increasing monotonously, with a small notch at the W mass and a less noticeable one at the Z mass. Note that for this value of m_1 (10GeV), all values reached by $\eta_{01}^{(4)}$ in the mass range considered, however large or small with respect to $\lambda_0^{(4)}$, are perturbatively acceptable.

Increasing m_1 to moderate values does not change the above qualitative features. As an illustration, Fig. 2 shows the behavior of $\eta_{01}^{(4)}$ as a function of m_0 for $m_1 = 30\text{GeV}$, keeping the mixing angle $\theta = 10^\circ$, still small, and the mutual S_0 – Higgs coupling constant

$$\theta = 10^\circ, \lambda_0^{(4)} = 0.01, m_0 = 1.4\text{GeV(L)} \text{ and } 1.5\text{GeV(R)}$$

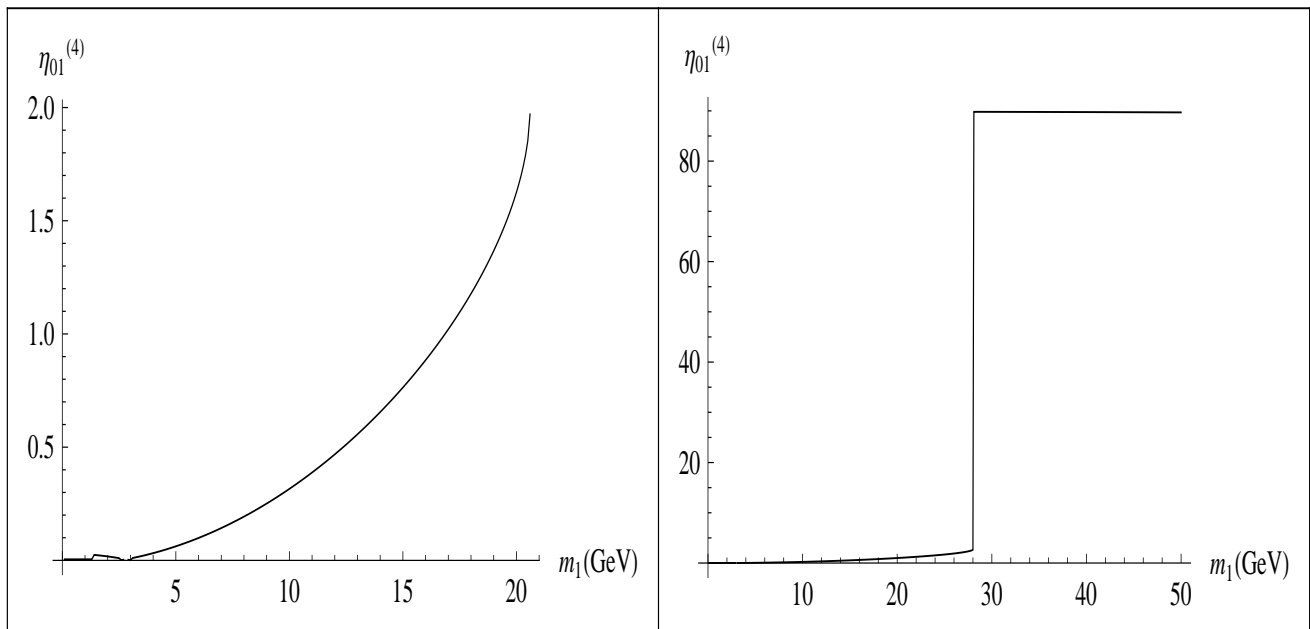


FIG. 4: $\eta_{01}^{(4)}$ versus m_1 for m_0 above τ threshold.

$\lambda_0^{(4)} = 0.01$, still very weak. The first thing to note is that not all values of $\eta_{01}^{(4)}$ are perturbative. Indeed, $\eta_{01}^{(4)}$ does not start until $m_0 \simeq 1.5\text{GeV}$, but with the very large value[†] 89.8. It decreases very sharply right after, to 2.04 at about 1.6GeV. It continues to decrease with a pronounced change in the slope at the b threshold. Effects at the masses $m_1/2$ and m_1 similar to those of figure 1 do occur here too. There is a desert that lies in this case in the mass interval 66.5GeV – 76.5GeV. At the upper bound, the coupling $\eta_{01}^{(4)}$ takes the value 2.15 and decreases very slowly till $m_0 \simeq 78.2\text{GeV}$. Right after this mass, it plunges down to catch up with a solution branch that is just emerging from negative values. This solution branch increases steadily with two small notches at the W and Z masses. A similar global behavior occurs at other moderate m_1 masses, with varying local features.

Because of the very-small- m_0 deserts described and visible on Fig. 1, one may ask whether the model ever allows for very light dark matter. To look into this, we fix m_0 at small values and let m_1 vary. Take first $m_0 = 0.2\text{GeV}$ and see Fig. 3. The allowed S_0 annihilation channels are the very light fermions e, u, d, μ and s , plus S_1 when $m_1 < m_0$.

[†] This feature is not displayed in figure 2 to avoid masking the other much smaller values taken by the mutual coupling.

$$\theta = 10^\circ, \lambda_0^{(4)} = 0.2, m_1 = 20\text{GeV}$$

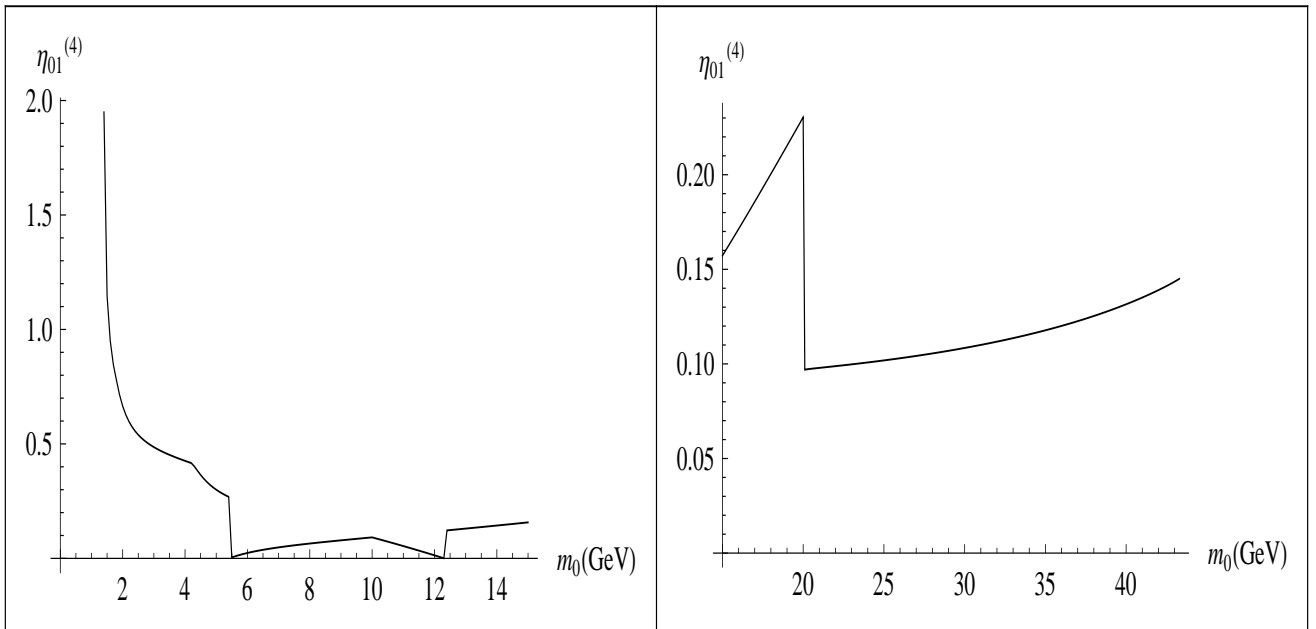


FIG. 5: $\eta_{01}^{(4)}$ vs m_0 for small mixing, moderate m_1 and WIMP-Higgs coupling.

Note that we still have $\theta = 10^\circ$ and $\lambda_0^{(4)} = 0.01$. Qualitatively, we notice that in fact, there are no solutions for $m_1 < 0.2\text{GeV}$ ($= m_0$ here), a mass at which $\eta_{01}^{(4)}$ takes the very small value $\simeq 0.003$. It goes up a solution branch and leaves it at $m_1 \simeq 0.4\text{GeV}$ to descend on a second branch that enters negative territory at $m_1 \simeq 0.7\text{GeV}$, forcing $\eta_{01}^{(4)}$ to return onto the first branch. There is an accelerated increase till $m_1 \simeq 5\text{GeV}$, a value at which $\eta_{01}^{(4)} \simeq 0.5$. And then a desert, no positive real solutions, no viable dark matter.

Increasing m_0 until about 1.3GeV does not change these overall features: some ‘movement’ for very small values of m_1 and then an accelerated increase till reaching a desert with a lower bound that changes with m_0 . For example, the desert starts at $m_1 \simeq 6.8\text{GeV}$ for $m_0 = 0.6\text{GeV}$ and $m_1 \simeq 7.3\text{GeV}$ for $m_0 = 1.2\text{GeV}$. Note that in all these cases where $m_0 \lesssim 1.3\text{GeV}$, all values of $\eta_{01}^{(4)}$ are perturbative. Therefore, the model can very well accommodate very light dark matter with a restricted range of S_1 masses.

However, the situation changes after the inclusion of the τ annihilation channel. Indeed, as Fig. 4 shows, for $m_0 = 1.4\text{GeV}$, though the overall shape of the behavior of $\eta_{01}^{(4)}$ as a function of m_1 is qualitatively the same, the desert threshold is pushed significantly higher, to $m_1 \simeq 20\text{GeV}$. But more significantly, $\eta_{01}^{(4)}$ starts to be larger than one already at $m_1 \simeq 17\text{GeV}$, therefore losing perturbativity. For $m_0 = 1.5\text{GeV}$, the desert is effectively erased as we have a sudden jump to highly non-perturbative values of $\eta_{01}^{(4)}$ right after $m_1 \simeq 28\text{GeV}$. Such a behavior stays with larger values of m_0 . But for $m_1 \lesssim 20\text{GeV}$ (case

$m_0 = 1.5\text{GeV}$), the values of $\eta_{01}^{(4)}$ are smaller than one and physical use of the model is possible if needed.

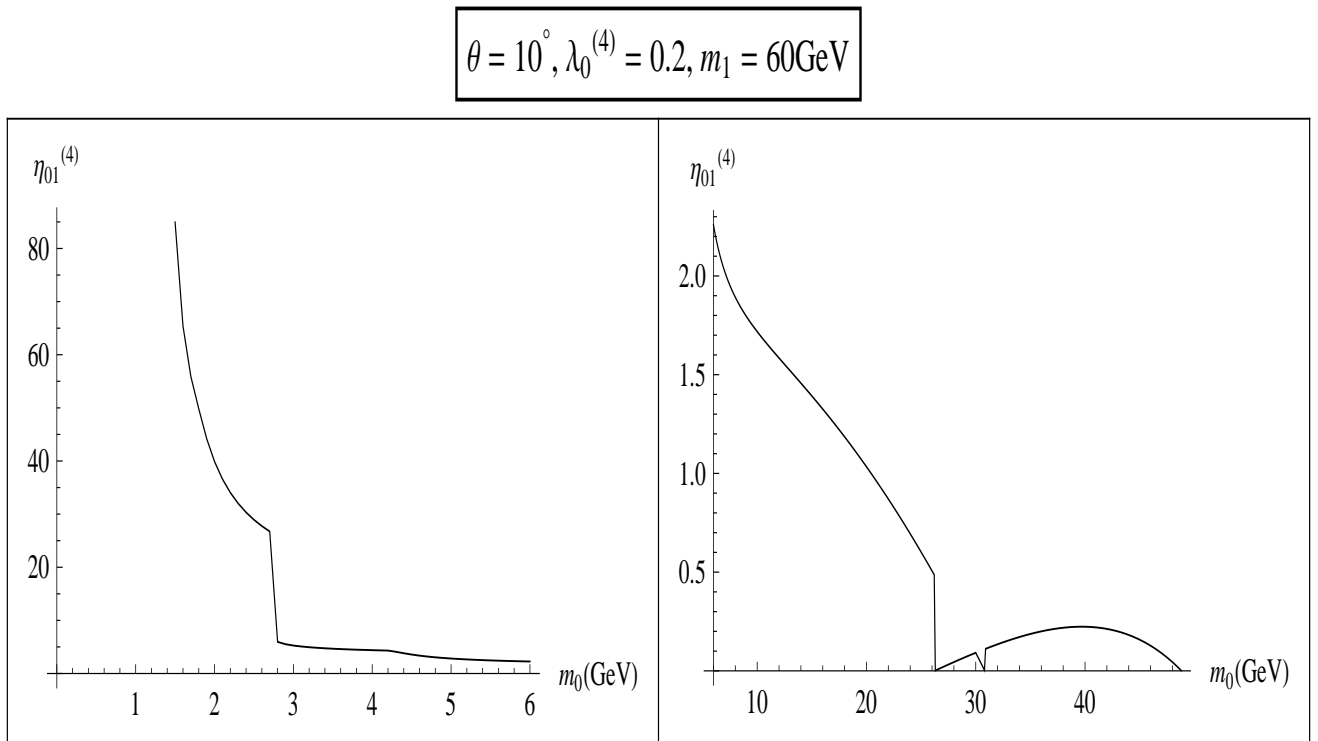


FIG. 6: $\eta_{01}^{(4)}$ versus m_0 for heavy S_1 , small mixing and small WIMP-Higgs coupling.

B. Small mixing angle and larger dark matter – Higgs couplings

What are the effects of the relic-density constraint when we vary the parameter $\lambda_0^{(4)}$? Let us keep the Higgs – S_1 mixing angle small ($\theta = 10^\circ$) and increase $\lambda_0^{(4)}$, first to 0.2 and later to 1. For $\lambda_0^{(4)} = 0.2$, Figure 5 shows the behavior of $\eta_{01}^{(4)}$ as a function of the dark matter mass m_0 when $m_1 = 20\text{GeV}$. We see that $\eta_{01}^{(4)}$ starts at $m_0 \simeq 1.4\text{GeV}$ with a value of about 1.95. It decreases with a sharp change of slope at the b threshold, then makes a sudden dive at about 5 GeV, a change of branch at $m_1/2$ down till about 12GeV where it jumps up back onto the previous branch just before going to cross into negative territory. It drops sharply at $m_0 = m_1$ and then increases slowly until $m_0 \simeq 43.3\text{GeV}$. Beyond, there is nothing, a desert.

This is of course different from the situation of very small $\lambda_0^{(4)}$ like in Fig. 1 and Fig. 2 above: here we see some kind of natural dark-matter mass ‘confinement’ to small-moderate

viable[‡] values.

Still for $\lambda_0^{(4)} = 0.2$ with $m_1 = 60\text{GeV}$ this time, Fig. 6 shows $\eta_{01}^{(4)}$ starting very high ($\simeq 85\text{GeV}$) at $m_0 \simeq 1.5\text{GeV}$, decreasing quickly with a first sudden drop at 2.7 GeV and a second one to zero at 26.2 GeV. A solution branch is then picked up – left briefly at $m_1/2$ – until 49 GeV and then nothing. What is peculiar here is that, in contrast with previous situations, the desert starts at a mass $m_0 < m_1$, i.e., before the opening of the S_1 annihilation channel. In other words, the dark matter is annihilating into the light fermions only and the model is perturbatively viable in the range 20GeV – 49GeV.

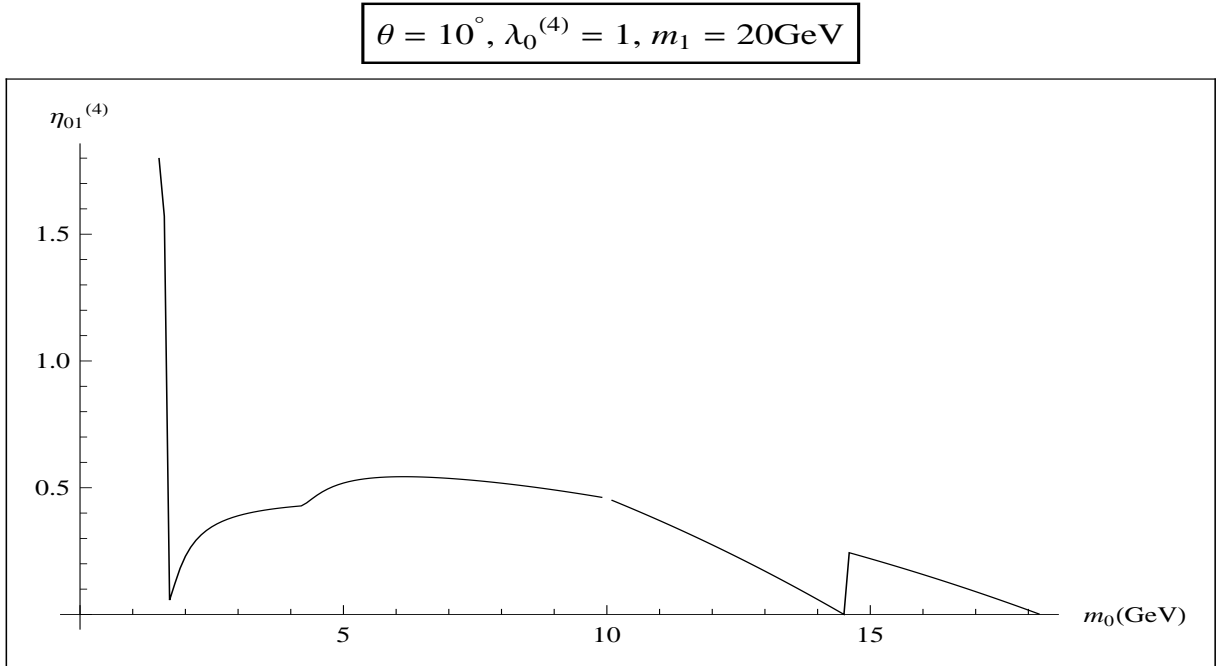


FIG. 7: $\eta_{01}^{(4)}$ versus m_0 for medium m_1 , small mixing and large WIMP-higgs coupling.

The case $\lambda_0^{(4)} = 1$ with $m_1 = 20\text{GeV}$ is displayed in Fig. 7. There are no solutions below $m_0 \simeq 1.5\text{GeV}$ at which $\eta_{01}^{(4)} \simeq 1.80$. From this value, $\eta_{01}^{(4)}$ slips down very quickly to pick up less abruptly when crossing the τ threshold. There is a significant change in the slope at the crossing of the b mass. Note the absence of a solution at $m_1/2$, which is a new feature, present for other values of m_1 not displayed here. Beyond $m_1/2$, there is a slight change in the downward slope, a change of solution branch, and that goes until 14.5GeV where $\eta_{01}^{(4)}$ jumps to catch up with the previous branch. It goes down this branch until about 18GeV where the desert starts.

We have studied the behavior of $\eta_{01}^{(4)}$ as a function of m_0 for other values of m_1 between 20GeV and 100GeV while keeping $\theta = 10^\circ$ and $\lambda_0^{(4)} = 1$. For $m_1 \lesssim 79.2\text{GeV}$, the behavior

[‡] Note that the values of $\eta_{01}^{(4)}$ for $1.6\text{GeV} \lesssim m_0 \lesssim 43.3\text{GeV}$ are all perturbative.

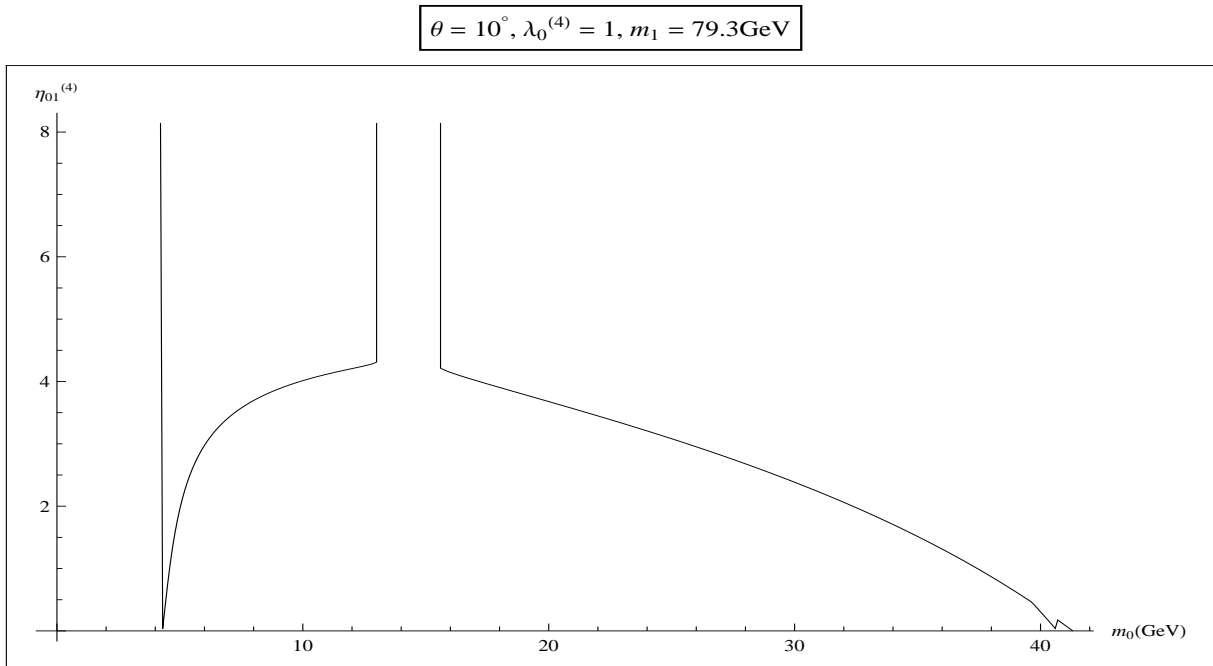


FIG. 8: $\eta_{01}^{(4)}$ versus m_0 for heavy S_1 , small mixing and large WIMP-Higgs coupling.

is qualitatively quite similar to that shown in Fig. 7, but beyond this mass, there is a highly non-perturbative branch $\eta_{01}^{(4)}$ jumps onto at small and moderate values of m_0 . This highly non-perturbative region stretches in size as m_1 increases. Fig. 8 displays this new feature. Note that on this figure, not all of the range of $\eta_{01}^{(4)}$ is shown in order to allow the small-coupling regions to be displayed; the high values of $\eta_{01}^{(4)}$ are in the two thousands. Note also that it is the same highly non-perturbative solution branch $\eta_{01}^{(4)}$ jumps onto for other large values of m_1 .

C. Larger mixing angles

Last in this descriptive study is to see the effects of larger values of the S_1 – Higgs mixing angle θ . We give it here the value $\theta = 40^\circ$ and tune back the mutual S_0 – Higgs coupling constant $\lambda_0^{(4)}$ to the very small value 0.01. Figure 9 shows the behavior of $\eta_{01}^{(4)}$ as a function of m_0 for $m_1 = 20\text{GeV}$. One recognizes features similar to those of the case $\theta = 10^\circ$, though coming in different relative sizes. The very-small- m_0 desert ends at about 0.3GeV. There are by-now familiar features at the c and b masses, $m_1/2$ and m_1 . Two relatively small forbidden intervals (deserts) appear for relatively large values of the dark matter mass: 67.3GeV – 70.9GeV and 79.4GeV – 90.8GeV. The W mass region is forbidden but there is action as we cross the Z mass.

Other values of m_1 , not displayed because of space, behave similarly with an additional

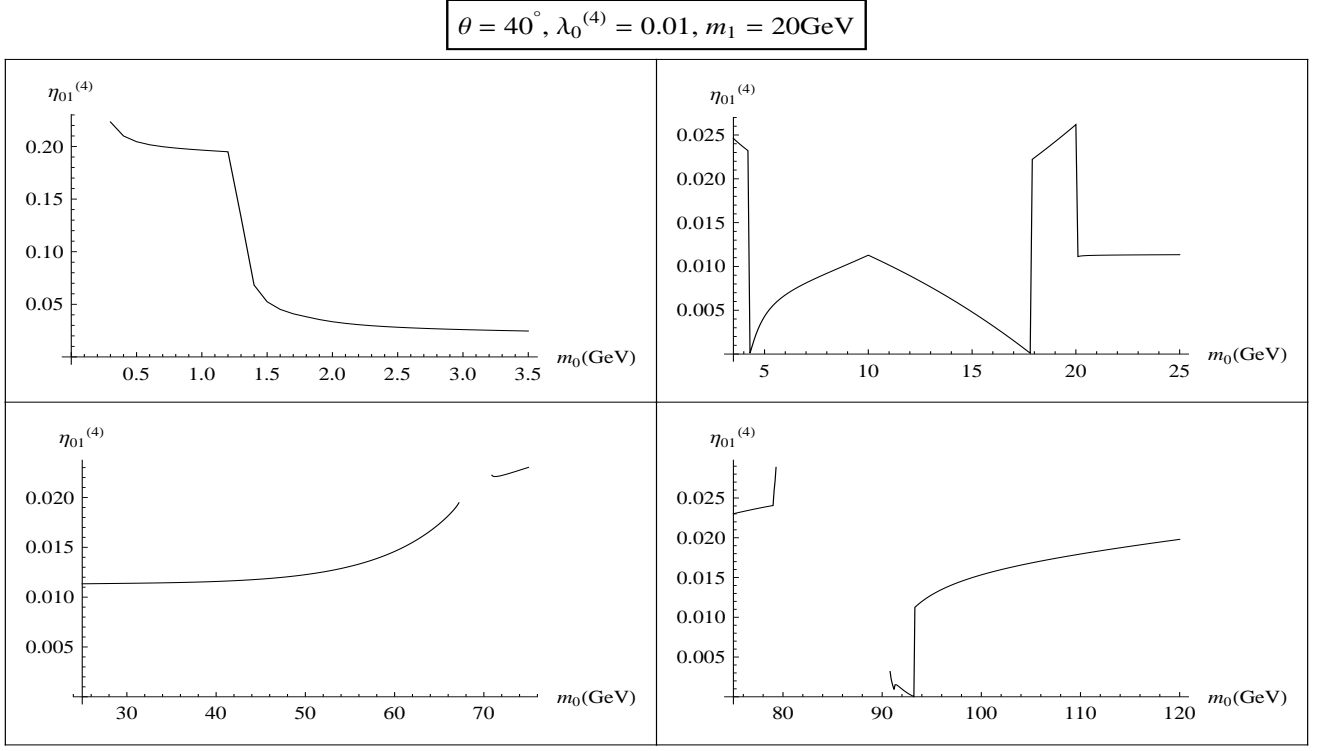


FIG. 9: $\eta_{01}^{(4)}$ versus m_0 for moderate m_1 , moderate mixing and small WIMP-Higgs coupling.

effect, namely, a sudden drop in slope at $m_0 = (m_h + m_1)/2$ coming from the ignition of S_0 annihilation into S_1 and Higgs. We have also worked out the cases $\lambda_0^{(4)} = 0.2$ and 1 for $\theta = 40^\circ$. The case $\lambda_0^{(4)} = 0.2$ is displayed in Fig. 10 and presents differences with the corresponding small-mixing situation $\theta = 10^\circ$. Indeed, for $m_1 = 20\text{GeV}$, the first feature we notice is a smoother behavior; compare with Fig. 5. Here, $\eta_{01}^{(4)}$ starts at $m_0 \simeq 0.3\text{GeV}$ with the small value $\simeq 0.016$ and goes up, faster at the c mass and with a small effect at the b mass. It increases very slowly until $m_1/2$ and decreases very slowly until $m_0 = m_1$, and then there is a sudden change of branch followed immediately by a desert[§]. So here too the model naturally confines the mass of a viable dark matter to small-moderate values, a dark matter particle annihilating into light fermions only. What is also noticeable is that there is stability of $\eta_{01}^{(4)}$ around the value of $\lambda_0^{(4)}$ in the interval $1.5\text{GeV} - 20\text{GeV}$ ($= m_1$ here).

The case $m_1 = 60\text{GeV}$ presents also overall similarities as well as noticeable differences with the corresponding case $\theta = 10^\circ$, see Fig. 6. The first difference is that all values of $\eta_{01}^{(4)}$ are perturbative. This latter starts at $m_0 \simeq 1.4\text{GeV}$ with the value ~ 0.75 , goes down and jumps to catch up with another solution branch emerging from negative territory when

[§] Except for the very tiny interval $78.5\text{GeV} - 79.0\text{GeV}$ not displayed on Fig. 10.

$$\theta = 40^\circ, \lambda_0^{(4)} = 0.2, m_1 = 20\text{GeV(L)} \text{ and } 60\text{GeV(R)}$$

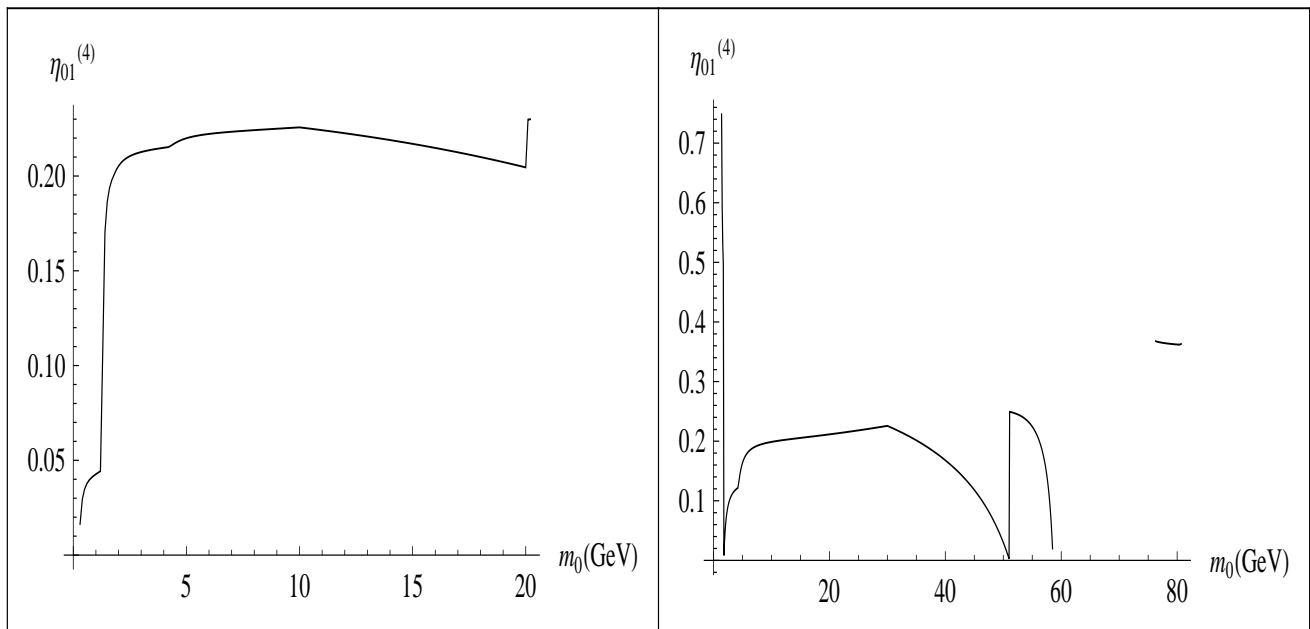


FIG. 10: $\eta_{01}^{(4)}$ versus m_0 for moderate (L) and large (R) m_1 , large mixing and moderate WIMP-Higgs coupling.

crossing the τ mass. It increases, kicking up when crossing the b -quark mass. It changes slope down at $m_1/2$ and goes to zero at about 51GeV. It jumps up onto another branch that goes down to zero also at about 58.6GeV, just below m_1 , and then there is a desert, except for the small interval 76.3GeV – 80.5GeV.

The case $\lambda_0^{(4)} = 1$ is shown in Fig. 11. Global similarities with the previous case are apparent. All values of $\eta_{01}^{(4)}$ are perturbative and the mass range is naturally confined to the interval 0.2GeV – 20GeV for $m_1 = 20$ GeV, and 1.4GeV – 52.3GeV for $m_1 = 60$ GeV. We note action at the usual masses and, in particular, we see there are no solutions at $m_0 = m_1/2$ like in the case $\theta = 10^\circ$. We note here too the quasi-constancy of $\eta_{01}^{(4)}$ for most of the available range.

Finally, we note that we have worked out larger mixing angles, notably $\theta = 75^\circ$. In general, these cases do not display any new features worth discussing: the overall behavior is mostly similar to what we have seen, with expected relative variations in size.

$$\theta = 40^\circ, \lambda_0^{(4)} = 1, m_1 = 20\text{GeV(L)} \text{ and } 60\text{GeV(R)}$$

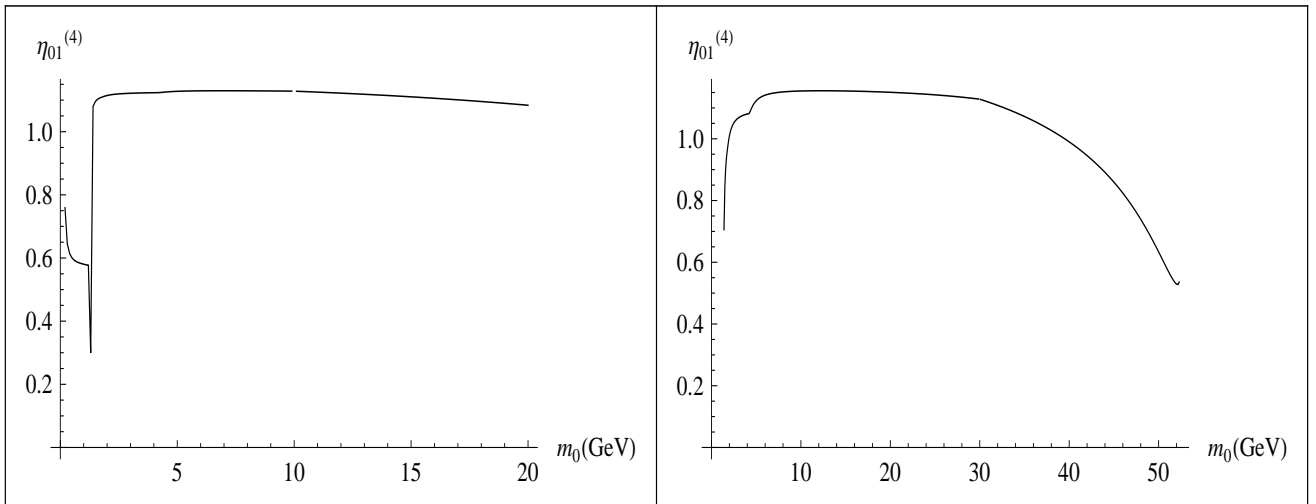


FIG. 11: $\eta_{01}^{(4)}$ versus m_0 for moderate (L) and large (R) m_1 , large mixing and large WIMP-Higgs coupling.

IV. DARK-MATTER DIRECT DETECTION

Experiments like CDMS II [27], XENON 10/100 [8, 26], DAMA/LIBRA [2] and CoGeNT [3] search directly for a dark matter signal. Such a signal would typically come from the elastic scattering of a dark matter WIMP off a non-relativistic nucleon target. However, throughout the years, such experiments have not yet detected an unambiguous signal, but rather yielded increasingly stringent exclusion bounds on the dark matter – nucleon elastic-scattering total cross section σ_{det} in terms of the dark matter mass m_0 .

In order for a theoretical dark-matter model to be viable, it has to satisfy these bounds. It is therefore natural to inquire whether the model we present in this work has any capacity of describing dark matter. Hence, we have to calculate σ_{det} as a function of m_0 for different values of the parameters $(\theta, \lambda_0^{(4)}, m_1)$ and project its behavior against the experimental bounds. We will limit ourselves to the region $0.1\text{GeV} - 100\text{GeV}$ as we are interested in light dark matter. As experimental bounds, we will use the results from CDMSII and XENON100, as well as the future projections of SuperCDMS [28] and XENON1T [29]. The results of CoGeNT, DAMA/LIBRA and CRESST will be discussed elsewhere [35]. As the figures below show [36], in the region of our interest, XENON100 is only slightly tighter than CDMSII, SuperCDMS significantly lower and XENON1T the most stringent by far. But it is important to note that all these results lose reasonable predictability in the very light sector, say below 5 GeV.

The scattering of S_0 off a SM fermion f occurs via the t-channel exchange of the SM higgs and S_1 . In the non-relativistic limit, the effective Lagrangian describing this

interaction reads

$$\mathcal{L}_{S_0-f}^{(eff)} = a_f \bar{f} f S_0^2, \quad (4.1)$$

where

$$a_f = -\frac{m_f}{2v} \left[\frac{\lambda_0^{(3)} \cos \theta}{m_h^2} - \frac{\eta_{01}^{(3)} \sin \theta}{m_1^2} \right]. \quad (4.2)$$

In this case the total cross section for this process is given by :

$$\sigma_{S_0 f \rightarrow S_0 f} = \frac{m_f^4}{4\pi (m_f + m_0)^2 v^2} \left[\frac{\lambda_0^{(3)} \cos \theta}{m_h^2} - \frac{\eta_{01}^{(3)} \sin \theta}{m_1^2} \right]^2. \quad (4.3)$$

At the nucleon level, the effective interaction between a nucleon $N = p$ or n and S_0 has the form

$$\mathcal{L}_{S_0-N}^{(eff)} = a_N \bar{N} N S_0^2, \quad (4.4)$$

where the effective nucleon- S_0 coupling constants is given by:

$$a_N = \frac{(m_N - \frac{7}{9}m_B)}{v} \left[\frac{\lambda_0^{(3)} \cos \theta}{m_h^2} - \frac{\eta_{01}^{(3)} \sin \theta}{m_1^2} \right]. \quad (4.5)$$

In this relation, m_N is the nucleon mass and m_B the baryon mass in the chiral limit [25]. The total cross section for non-relativistic $S_0 - N$ elastic scattering is therefore:

$$\sigma_{\text{det}} \equiv \sigma_{S_0 N \rightarrow S_0 N} = \frac{m_N^2 (m_N - \frac{7}{9}m_B)^2}{4\pi (m_N + m_0)^2 v^2} \left[\frac{\lambda_0^{(3)} \cos \theta}{m_h^2} - \frac{\eta_{01}^{(3)} \sin \theta}{m_1^2} \right]^2. \quad (4.6)$$

The rest of this section is devoted to a brief discussion of the behavior of σ_{det} as a function of m_0 . We will of course impose the relic-density constraint on the dark matter annihilation cross section (3.2). But in addition, we will require that the coupling constants are perturbative, and so impose the additional requirement $0 \leq \eta_{01}^{(4)} \leq 1$. Also, here too, the choices of the sets of values of the parameters $(\theta, \lambda_0^{(4)}, m_1)$ can by no means be exhaustive but only indicative. Furthermore, though a detailed description of the behavior of σ_{det} could be interesting in its own right, we will refrain from doing so in this work as there is no need for it, and content ourselves with mentioning overall features and trends. Generally, as m_0 increases, the detection cross section σ_{det} starts from high values, slopes down to minima that depend on the parameters and then picks up moderately. There are features and action at the usual mass thresholds, with varying sizes and shapes. Excluded regions are there, those coming from the relic-density constraint and new ones originating from the additional perturbativity requirement. Close to the upper boundary of the mass interval considered in this study, there is no universal behavior to mention as in some cases

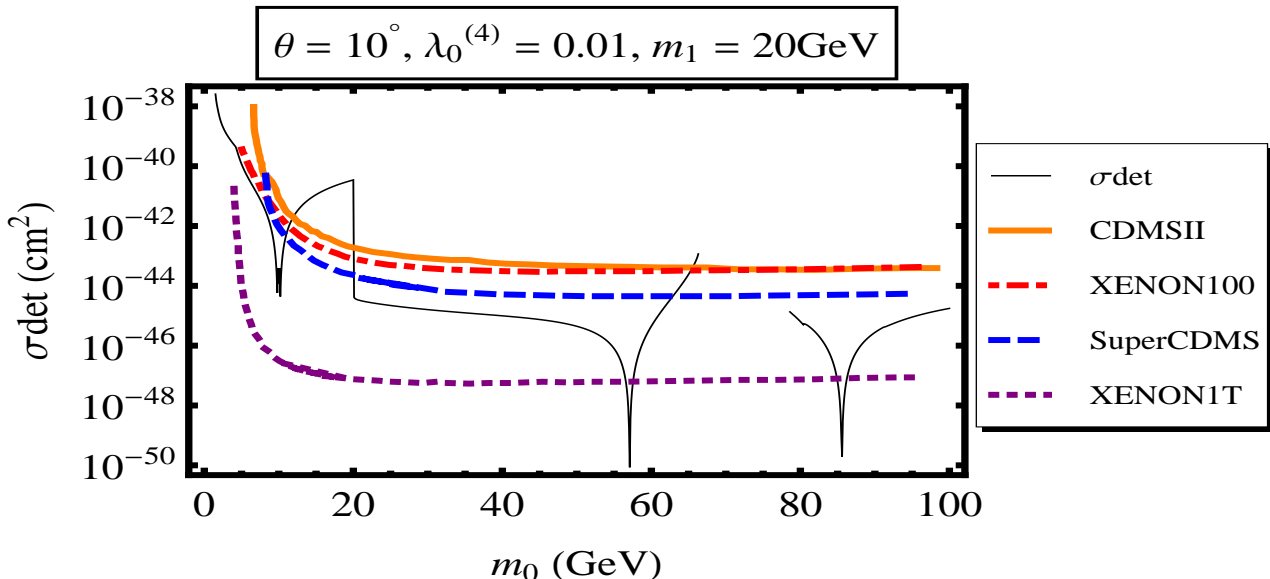


FIG. 12: Elastic $N - S_0$ scattering cross-section as a function of m_0 for moderate m_1 , small mixing and small WIMP-Higgs coupling.

σ_{det} will increase monotonously and, in some others, it will decrease or ‘not be there’ at all. Let us finally remark that the logplots below may not show these general features clearly as these latter are generally distorted.

Let us start with the small Higgs - S_1 mixing angle $\theta = 10^\circ$ and the very weak mutual $S_0 - \text{Higgs}$ coupling $\lambda_0^{(4)} = 0.01$. Fig. 12 shows the behavior of σ_{det} versus m_0 in the case $m_1 = 20\text{GeV}$. We see that for the two mass intervals $20\text{GeV} - 65\text{GeV}$ and $75\text{GeV} - 100\text{GeV}$, plus an almost singled-out peaks at $m_0 = m_1/2$, the elastic scattering cross section is below the projected sensitivity of SuperCDMS. However, XENON1T will probe all the these masses , except $m_0 \simeq 58 \text{ GeV}$ and 85 GeV .

Also, as we see in Fig. 12, most of the mass range for very light dark matter is excluded for these values of the parameters. Is this systematic? In general, smaller values of m_1 drive the predictability ranges to the lighter sector of the dark matter masses. Figure 13 illustrates this pattern. We have taken $m_1 = 5\text{GeV}$, just above the lighter quarks threshold. In the small-mass region, we see that SuperCDMS is passed in the range $5\text{GeV} - 30\text{GeV}$. Again , all this mass ranges will be probed by XENON1T experiment, except a sharp peak at $m_0 = m_1/2 = 2.5\text{GeV}$, but for such a very light mass, the experimental results are not without ambiguity.

Reversely, increasing m_1 shuts down possibilities for very light dark matter and thins the intervals as it drives the predicted masses to larger values. For instance, in figure 14 where $m_1 = 40\text{GeV}$, in addition to the peak at $m_1/2$ that crosses SuperCDMS but not XENON1T, we see acceptable masses in the ranges $40\text{GeV} - 65\text{GeV}$ and $78\text{GeV} - \text{up}$.

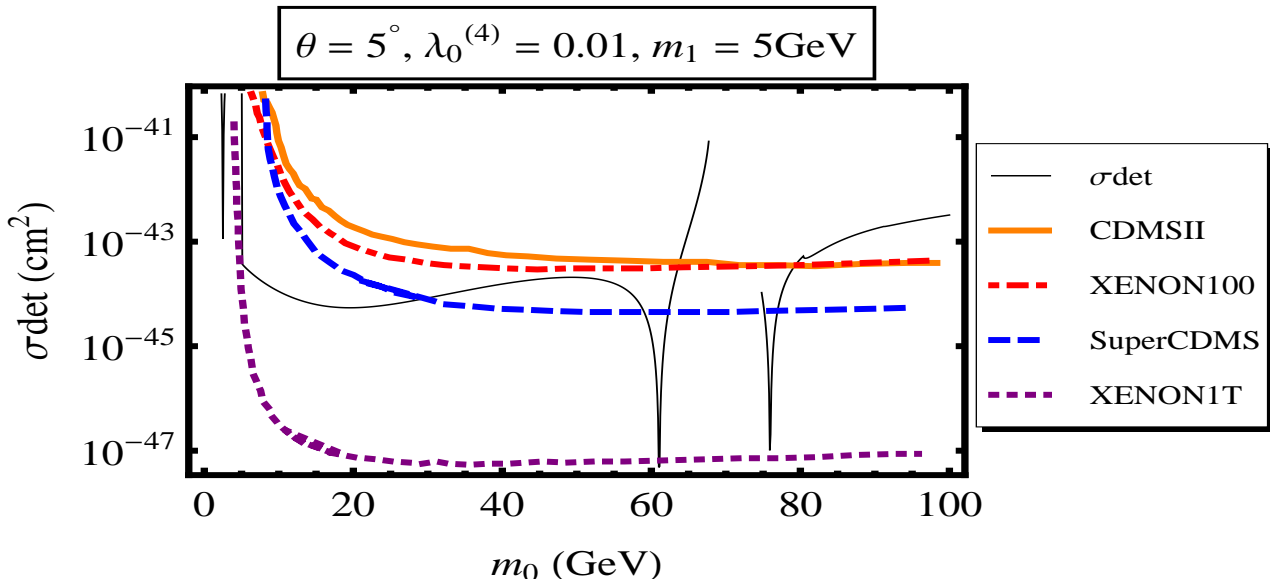


FIG. 13: *Elastic $N - S_0$ scattering cross-section as a function of m_0 for light S_1 , small mixing and small WIMP-Higgs coupling.*

Here too the intervals narrow as we descend, surviving XENON1T as spiked peaks at 62 GeV and around 95 GeV.

A larger mutual coupling constant $\lambda_0^{(4)}$ has the general effect of squeezing the acceptable intervals of m_0 by pushing the values of σ_{det} up. As an illustration, see figure 15 where we have taken $\lambda_0^{(4)} = 0.2$ and a larger value of $m_1 = 60\text{GeV}$. In this example, already XENON100 excludes all the masses below 100 GeV except a relatively narrow peak at $m_1/2$.

Increasing the mixing angle θ has also the general effect of increasing the value of σ_{det} . Figure 16 shows this trend for $\theta = 40^\circ$; compare with Fig. 12. The only allowed masses by the current bounds of CDMSII and XENON100 are between 20 GeV and 50 GeV, the narrow interval around $m_1/2$, and another very sharp one, at about 94 GeV. The projected sensitivity of XENON1T will probe all mass ranges except those at $m_0 \simeq 30\text{GeV}$ and 94 GeV.

Finally, it happens that there are regions of the parameters for which the model has no predictability. See figure 17 for illustration. We have combined the effects of increasing the values of the two parameters $\lambda_0^{(4)}$ and m_1 . As we see, we barely get something at $m_1/2$ that cannot even cross XENON100 down to SuperCDMS.

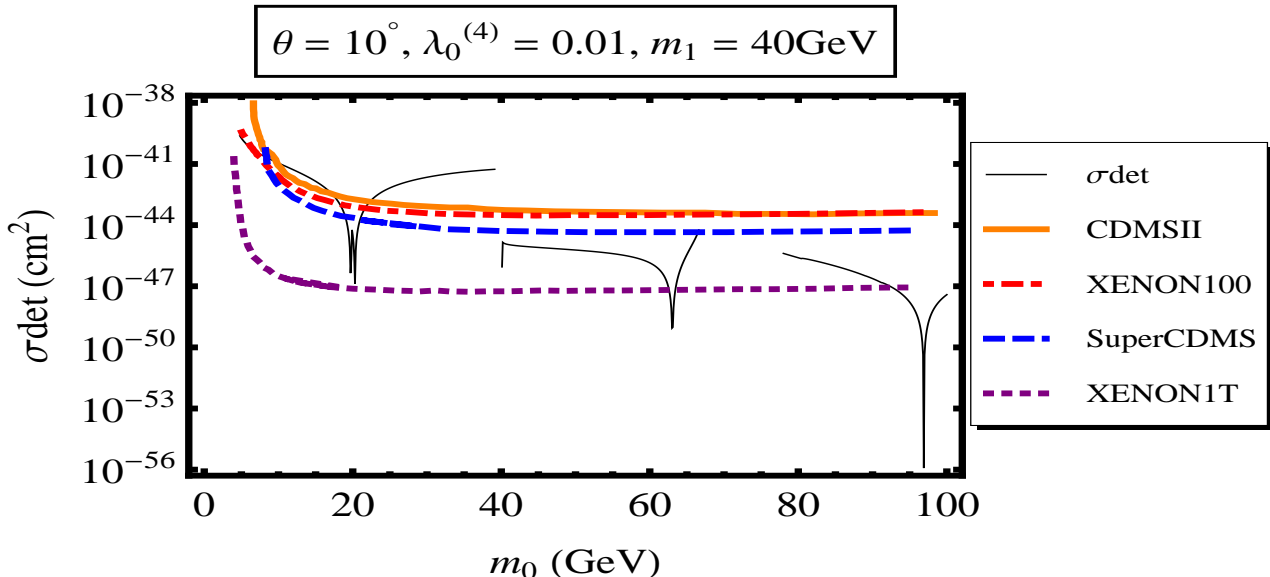


FIG. 14: *Elastic $N - S_0$ scattering cross-section as a function of m_0 for medium m_1 , small mixing and small WIMP-Higgs coupling.*

V. CONCLUDING REMARKS

In this work, we presented a plausible scenario for light cold dark matter, (for masses lighter than 100 GeV). This latter consists in enlarging the Standard Model with two gauge-singlet \mathbb{Z}_2 -symmetric scalar fields. One is the dark matter field S_0 , stable, while the other undergoes spontaneous symmetry breaking, resulting in the physical field S_1 . This opens additional channels through which S_0 can annihilate, hence a reducing its number density. The model is parametrized by three quantities: the physical mutual coupling constant $\lambda_0^{(4)}$ between S_0 and the Higgs, the mixing angle θ between S_1 and the Higgs and the mass m_1 of the particle S_1 . We first imposed on S_0 annihilation cross section the constraint from the observed dark-matter relic density and studied its effects through the behavior of the physical mutual coupling constant $\eta_{01}^{(4)}$ between S_0 and S_1 as a function of the dark matter mass m_0 . Apart from forbidden regions (deserts) or others where perturbativity is lost, we find that for most values of the three parameters, there are viable solutions in the small-moderate masses of the dark matter sector. Deserts are found for most of the ranges of the parameters whereas perturbativity is lost mainly for larger values of m_1 . Through the behavior of $\eta_{01}^{(4)}$, we could see the mass thresholds which mostly affect the annihilation of dark matter, and these are at the c , τ and b masses, as well as $m_1/2$ and m_1 .

The current experimental bounds from CDMSII and XENON100 put a strong constraint on the S_0 masses in the range between 10 to 20 GeV. For small values of m_1 , very light dark matter is viable, with a mass as small as one GeV. This is of course useful for

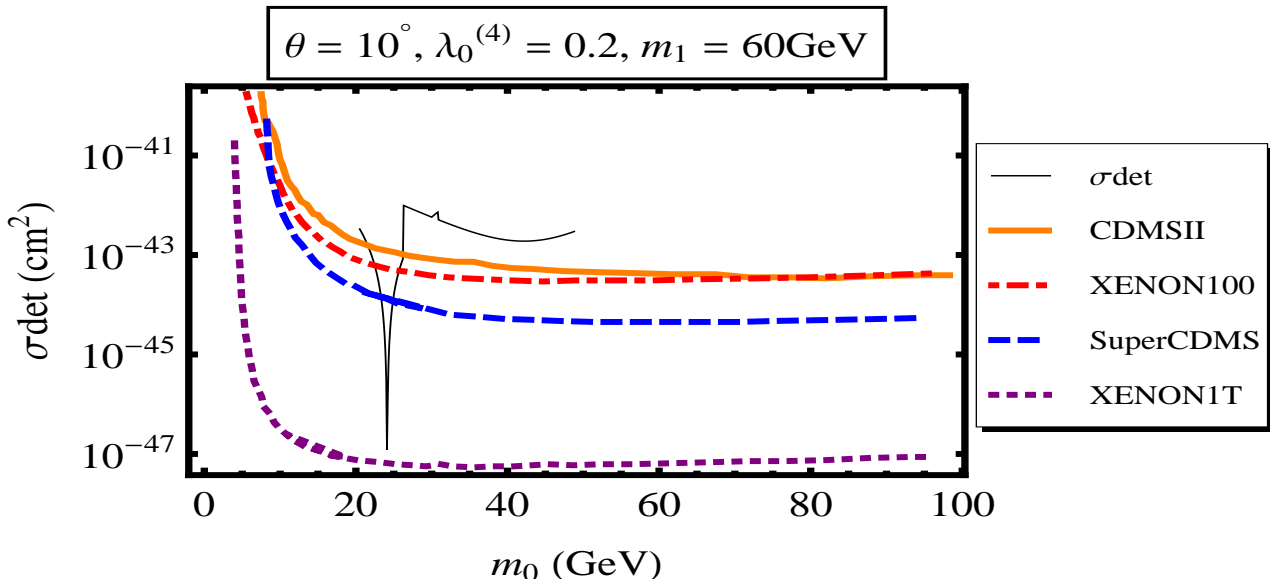


FIG. 15: *Elastic $N - S_0$ scattering cross-section as a function of m_0 for heavy S_1 , small mixing and moderate WIMP-Higgs coupling.*

understanding the results of the experiments DAMA/LIBRA, CoGeNT , CRESST [14] as well as the recent data of the Fermi Gamma Ray Space Telescope [4] . The projected sensitivity of future WIMP direct searches such as XENON1T will probe all the S_0 masses between 5 GeV and 100 GeV.

The next step to take is to test the model against the phenomenological constraints. Indeed, one important feature of the model is that it mixes the S_1 field with the Higgs. This must have implications on the Higgs detection through the measurable channels. Current experimental bounds from LEP II data can be used to constrain our mixing angle θ , and possibly other parameters. In addition, a very light S_0 and/or S_1 will contribute to the invisible decay of J/ψ and Υ mesons and can lead to a significant branching fraction. These constraints can be injected back into the model and restrain further its domain of validity. These issues are under current investigation [35].

Also, in this work, the S_1 vacuum expectation value v_1 was taken equal to 100GeV, but a priori, nothing prevents us from considering other scales. However, taking v_1 much larger than the electro-weak scale requires $\eta_{01}^{(4)}$ to be very tiny , which will result in the suppression of the crucial annihilation channel $S_0 S_0 \rightarrow S_1 S_1$. Also, we have fixed the Higgs mass to $m_h = 138\text{GeV}$, which is consistent with the current acceptable experimental bounds [30]. Yet, it can be useful to ask here too what the effect of changing this mass would be.

Finally, in this study, besides the dark matter field S_0 , only one extra field has been considered. Naturally, one can generalize the investigation to include N such fields and

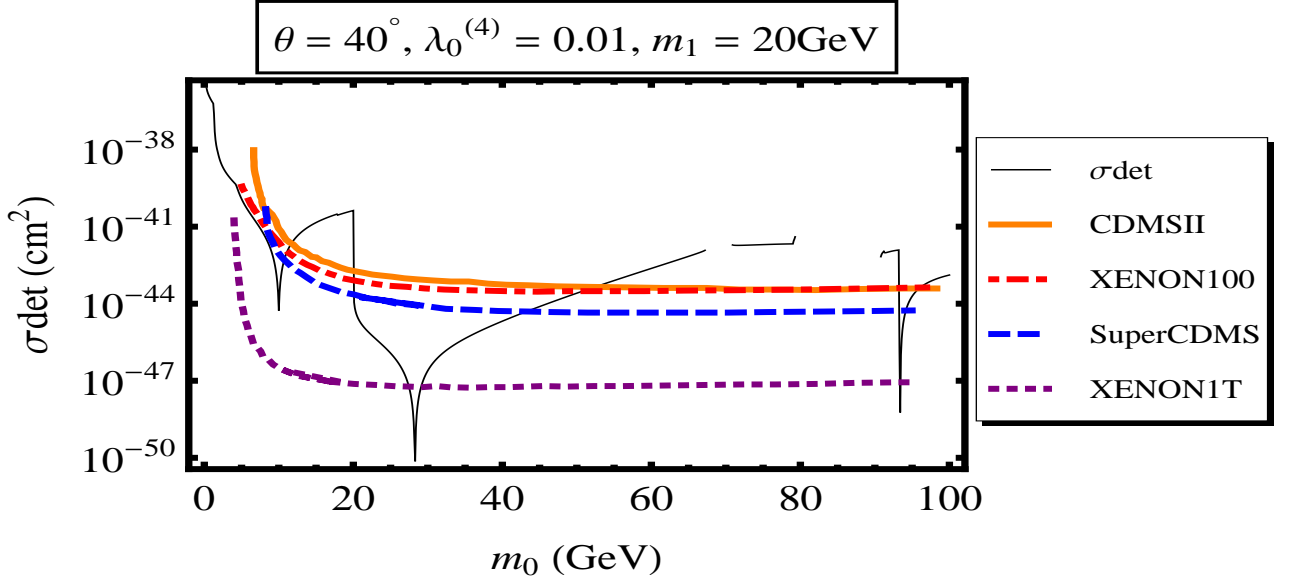


FIG. 16: *Elastic $N - S_0$ scattering cross-section as a function of m_0 for moderate m_1 , large mixing and small WIMP-Higgs coupling.*

discuss the cosmology and particle phenomenology in terms of N . It just happens that the model is rich enough to open new possibilities in the quest of dark matter worth pursuing.

Appendix A: Dark matter annihilation cross-sections

The cross-sections related to the annihilation S_0 into the scalar particles are as follows. For the hh channel, we have:

$$\begin{aligned}
v_{12}\sigma_{S_0 S_0 \rightarrow hh} = & \frac{\sqrt{m_0^2 - m_h^2}}{64\pi m_0^3} \Theta(m_0 - m_h) \left[\left(\lambda_0^{(4)} \right)^2 + \frac{4\lambda_0^{(4)} \left(\lambda_0^{(3)} \right)^2}{m_h^2 - 2m_0^2} + \frac{2\lambda_0^{(4)} \lambda_0^{(3)} \lambda^{(3)}}{4m_0^2 - m_h^2} \right. \\
& + \frac{2\lambda_0^{(4)} \lambda_1^{(3)} \eta_{01}^{(3)} (4m_0^2 - m_1^2)}{(4m_0^2 - m_1^2)^2 + \epsilon_1^2} + \frac{4 \left(\lambda_0^{(3)} \right)^4}{(m_h^2 - 2m_0^2)^2} + \frac{4\lambda^{(3)} \left(\lambda_0^{(3)} \right)^3}{(4m_0^2 - m_h^2)(m_h^2 - 2m_0^2)} \\
& + \frac{4 \left(\lambda_0^{(3)} \right)^2 \lambda_1^{(3)} \eta_{01}^{(3)} (4m_0^2 - m_1^2)}{[(4m_0^2 - m_1^2)^2 + \epsilon_1^2] (m_h^2 - 2m_0^2)} + \frac{(\lambda^{(3)})^2 \left(\lambda_0^{(3)} \right)^2}{(4m_0^2 - m_h^2)^2} \\
& \left. + \frac{\left(\lambda_1^{(3)} \right)^2 \left(\eta_{01}^{(3)} \right)^2}{(4m_0^2 - m_1^2)^2 + \epsilon_1^2} + \frac{2\lambda_0^{(3)} \lambda_1^{(3)} \lambda^{(3)} \eta_{01}^{(3)} (4m_0^2 - m_1^2)}{[(4m_0^2 - m_1^2)^2 + \epsilon_1^2] (4m_0^2 - m_h^2)} \right]. \quad (\text{A1})
\end{aligned}$$

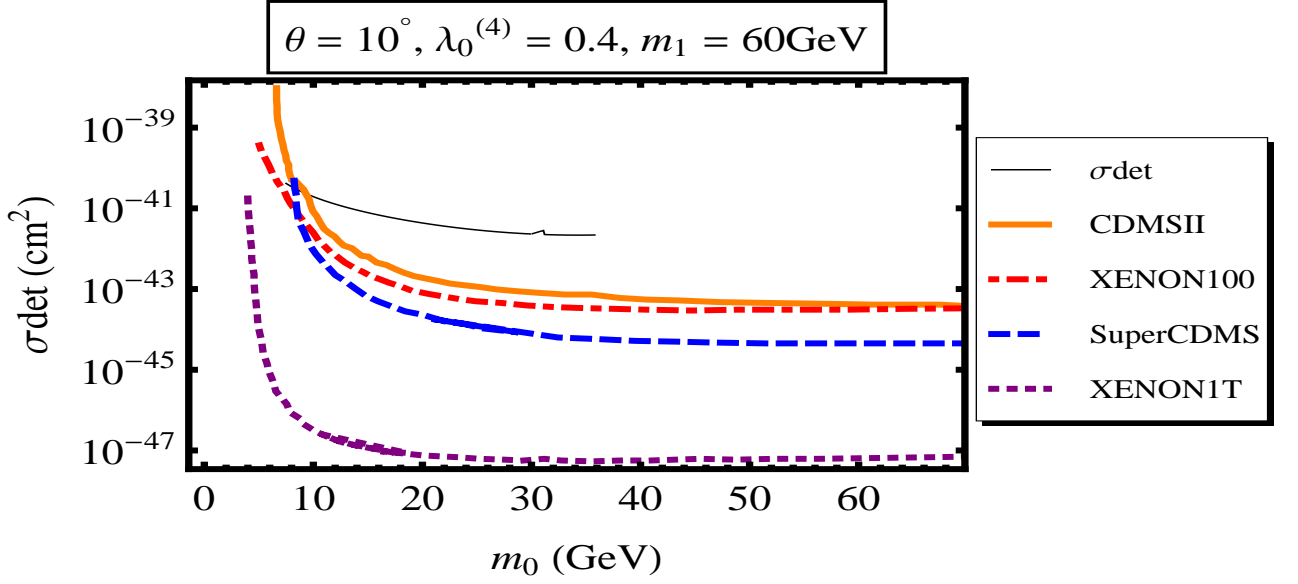


FIG. 17: elastic cross-section σ_{el} as a function of S_0 mass for heavy S_1 , small mixing and relatively large WIMP-Higgs coupling.

The Θ function is the step function. For the $S_1 S_1$ channel, we have the result:

$$\begin{aligned}
v_{12}\sigma_{S_0 S_0 \rightarrow S_1 S_1} = & \frac{\sqrt{m_0^2 - m_1^2}}{64\pi m_0^3} \Theta(m_0 - m_1) \left[\left(\eta_{01}^{(4)} \right)^2 + \frac{4\eta_{01}^{(4)} \left(\eta_{01}^{(3)} \right)^2}{m_1^2 - 2m_0^2} + \frac{2\eta_{01}^{(4)} \eta_{01}^{(3)} \eta_1^{(3)}}{4m_0^2 - m_1^2} \right. \\
& + \frac{2\eta_{01}^{(4)} \lambda_0^{(3)} \lambda_2^{(3)} (4m_0^2 - m_h^2)}{(4m_0^2 - m_h^2)^2 + \epsilon_h^2} + \frac{4 \left(\eta_{01}^{(3)} \right)^4}{(m_1^2 - 2m_0^2)^2} + \frac{4 \left(\eta_{01}^{(3)} \right)^3 \eta_1^{(3)}}{(4m_0^2 - m_1^2)(m_1^2 - 2m_0^2)} \\
& + \frac{4 \left(\eta_{01}^{(3)} \right)^2 \lambda_0^{(3)} \lambda_2^{(3)} (4m_0^2 - m_h^2)}{[(4m_0^2 - m_h^2)^2 + \epsilon_h^2] (m_1^2 - 2m_0^2)} + \frac{\left(\eta_{01}^{(3)} \right)^2 \left(\eta_1^{(3)} \right)^2}{(4m_0^2 - m_1^2)^2} \\
& \left. + \frac{\left(\lambda_0^{(3)} \right)^2 \left(\lambda_2^{(3)} \right)^2}{(4m_0^2 - m_h^2)^2 + \epsilon_h^2} + \frac{2\eta_{01}^{(3)} \eta_1^{(3)} \lambda_0^{(3)} \lambda_2^{(3)} (4m_0^2 - m_h^2)}{[(4m_0^2 - m_h^2)^2 + \epsilon_h^2] (4m_0^2 - m_1^2)} \right]. \quad (\text{A2})
\end{aligned}$$

For the hS_1 channel, we have:

$$\begin{aligned}
v_{12}\sigma_{S_0S_0\rightarrow S_1h} &= \frac{\sqrt{[4m_0^2 - (m_h - m_1)^2][4m_0^2 - (m_h + m_1)^2]}}{128\pi m_0^4} \Theta(2m_0 - m_h - m_1) \\
&\left[\left(\lambda_{01}^{(4)}\right)^2 + \frac{8\lambda_{01}^{(4)}\eta_{01}^{(3)}\lambda_0^{(3)}}{m_h^2 + m_1^2 - 4m_0^2} + \frac{2\lambda_{01}^{(4)}\lambda_0^{(3)}\lambda_1^{(3)}}{4m_0^2 - m_h^2} + \frac{2\lambda_{01}^{(4)}\eta_{01}^{(3)}\lambda_2^{(3)}}{4m_0^2 - m_1^2} \right. \\
&+ \frac{16\left(\eta_{01}^{(3)}\right)^2\left(\lambda_0^{(3)}\right)^2}{(m_h^2 + m_1^2 - 4m_0^2)^2} + \frac{8\left(\lambda_0^{(3)}\right)^2\eta_{01}^{(3)}\lambda_1^{(3)}}{(m_h^2 + m_1^2 - 4m_0^2)(4m_0^2 - m_h^2)} \\
&+ \frac{8\left(\eta_{01}^{(3)}\right)^2\lambda_0^{(3)}\lambda_2^{(3)}}{(m_h^2 + m_1^2 - 4m_0^2)(4m_0^2 - m_1^2)} + \frac{\left(\lambda_0^{(3)}\right)^2\left(\lambda_1^{(3)}\right)^2}{(4m_0^2 - m_h^2)^2} \\
&\left. + \frac{2\eta_{01}^{(3)}\lambda_0^{(3)}\lambda_1^{(3)}\lambda_2^{(3)}}{(4m_0^2 - m_h^2)(4m_0^2 - m_1^2)} + \frac{\left(\lambda_2^{(3)}\right)^2\left(\eta_{01}^{(3)}\right)^2}{(4m_0^2 - m_1^2)^2} \right]. \tag{A3}
\end{aligned}$$

The annihilation cross-section into fermions is:

$$\begin{aligned}
v_{12}\sigma_{S_0S_0\rightarrow f\bar{f}} &= \frac{\sqrt{(m_0^2 - m_f^2)^3}}{4\pi m_0^3} \Theta(m_0 - m_f) \left[\frac{\left(\lambda_0^{(3)}\lambda_{hf}\right)^2}{(4m_0^2 - m_h^2)^2 + \epsilon_h^2} + \frac{\left(\eta_{01}^{(3)}\lambda_{1f}\right)^2}{(4m_0^2 - m_1^2)^2 + \epsilon_1^2} \right. \\
&\left. + \frac{2\lambda_0^{(3)}\eta_{01}^{(3)}\lambda_{hf}\lambda_{1f}(4m_0^2 - m_h^2)(4m_0^2 - m_1^2)}{\left[(4m_0^2 - m_h^2)^2 + \epsilon_h^2\right]\left[(4m_0^2 - m_1^2)^2 + \epsilon_1^2\right]} \right]. \tag{A4}
\end{aligned}$$

The annihilation cross-section into W 's is given by:

$$\begin{aligned}
v_{12}\sigma_{S_0S_0\rightarrow WW} &= \frac{\sqrt{m_0^2 - m_w^2}}{16\pi m_0^3} \Theta(m_0 - m_w) \left[1 + \frac{(2m_0^2 - m_w^2)^2}{2m_w^4} \right] \\
&\times \left[\frac{\left(\lambda_0^{(3)}\lambda_{hw}\right)^2}{(4m_0^2 - m_h^2)^2 + \epsilon_h^2} + \frac{\left(\eta_{01}^{(3)}\lambda_{1w}\right)^2}{(4m_0^2 - m_1^2)^2 + \epsilon_1^2} \right. \\
&\left. + \frac{2\lambda_0^{(3)}\eta_{01}^{(3)}\lambda_{hw}\lambda_{1w}(4m_0^2 - m_h^2)(4m_0^2 - m_1^2)}{\left[(4m_0^2 - m_h^2)^2 + \epsilon_h^2\right]\left[(4m_0^2 - m_1^2)^2 + \epsilon_1^2\right]} \right]. \tag{A5}
\end{aligned}$$

Last, the annihilation cross-section into Z 's is:

$$\begin{aligned}
v_{12}\sigma_{S_0S_0\rightarrow ZZ} &= \frac{\sqrt{m_0^2 - m_z^2}}{8\pi m_0^3} \Theta(m_0 - m_z) \left[1 + \frac{(2m_0^2 - m_z^2)^2}{2m_z^4} \right] \\
&\times \left[\frac{(\lambda_0^{(3)}\lambda_{hz}^{(3)})^2}{(4m_0^2 - m_h^2)^2 + \epsilon_h^2} + \frac{(\eta_{01}^{(3)}\lambda_{1z}^{(3)})^2}{(4m_0^2 - m_1^2)^2 + \epsilon_1^2} \right. \\
&\left. + \frac{2\lambda_0^{(3)}\eta_{01}^{(3)}\lambda_{hz}^{(3)}\lambda_{1z}^{(3)}(4m_0^2 - m_h^2)(4m_0^2 - m_1^2)}{[(4m_0^2 - m_h^2)^2 + \epsilon_h^2][(4m_0^2 - m_1^2)^2 + \epsilon_1^2]} \right]. \tag{A6}
\end{aligned}$$

The quantities $\epsilon_h = m_h\Gamma_h$ and $\epsilon_1 = m_1\Gamma_1$ are regulators at the respective resonances. The decay rates Γ_h and Γ_1 are calculable in perturbation theory. We have for h :

$$\begin{aligned}
\epsilon_{h\rightarrow f\bar{f}} &= \frac{(\lambda_{hf})^2}{8\pi} m_h^2 N_c \left(1 - \frac{4m_f^2}{m_h^2} \right)^{\frac{3}{2}} \Theta(m_h - 2m_f); \\
\epsilon_{h\rightarrow WW} &= \frac{(\lambda_{hw}^{(3)})^2}{8\pi} \left(1 - \frac{4m_w^2}{m_h^2} \right)^{\frac{1}{2}} \left[1 + \frac{(m_h^2 - 2m_w^2)^2}{8m_w^4} \right] \Theta(m_h - 2m_w); \\
\epsilon_{h\rightarrow ZZ} &= \frac{(\lambda_{hz}^{(3)})^2}{4\pi} \left(1 - \frac{4m_z^2}{m_h^2} \right)^{\frac{1}{2}} \left[1 + \frac{(m_h^2 - 2m_z^2)^2}{8m_z^4} \right] \Theta(m_h - 2m_z); \\
\epsilon_{h\rightarrow S_0S_0} &= \frac{(\lambda_0^{(3)})^2}{32\pi} \left(1 - \frac{4m_0^2}{m_h^2} \right)^{\frac{1}{2}} \Theta(m_h - 2m_0); \\
\epsilon_{h\rightarrow S_1S_1} &= \frac{(\lambda_2^{(3)})^2}{32\pi} \left(1 - \frac{4m_1^2}{m_h^2} \right)^{\frac{1}{2}} \Theta(m_h - 2m_1). \tag{A7}
\end{aligned}$$

For S_1 , we have similar expressions:

$$\begin{aligned}
\epsilon_{S_1 \rightarrow f\bar{f}} &= \frac{(\lambda_{1f})^2}{8\pi} m_1^2 N_c \left(1 - \frac{4m_f^2}{m_1^2}\right)^{\frac{3}{2}} \Theta(m_1 - 2m_f); \\
\epsilon_{S_1 \rightarrow WW} &= \frac{(\lambda_{1w}^{(3)})^2}{8\pi} \left(1 - \frac{4m_w^2}{m_1^2}\right)^{\frac{1}{2}} \left[1 + \frac{(m_1^2 - 2m_w^2)^2}{8m_w^4}\right] \Theta(m_1 - 2m_w); \\
\epsilon_{S_1 \rightarrow ZZ} &= \frac{(\lambda_{1z}^{(3)})^2}{4\pi} \left(1 - \frac{4m_z^2}{m_1^2}\right)^{\frac{1}{2}} \left[1 + \frac{(m_1^2 - 2m_z^2)^2}{8m_z^4}\right] \Theta(m_1 - 2m_z); \\
\epsilon_{S_1 \rightarrow S_0 S_0} &= \frac{(\eta_{01}^{(3)})^2}{32\pi} \left(1 - \frac{4m_0^2}{m_1^2}\right)^{\frac{1}{2}} \Theta(m_1 - 2m_0); \\
\epsilon_{S_1 \rightarrow hh} &= \frac{(\lambda_1^{(3)})^2}{32\pi} \left(1 - \frac{4m_h^2}{m_1^2}\right)^{\frac{1}{2}} \Theta(m_1 - 2m_h). \tag{A8}
\end{aligned}$$

where N_c is equal to 1 for leptons and 3 for quarks.

-
- [1] D. N. Spergel *et al.* [WMAP Collaboration], *Astrophys. J. Suppl.* **170** (2007) 377 ([arXiv:astro-ph/0603449].); A. C. Pope *et al.* [The SDSS Collaboration], *Astrophys. J.* **607** (2004) 655 (arXiv:astro-ph/0401249).
- [2] R. Bernabei, P. Belli and F. Cappella *et al.* [DAMA/LIBRA Collaboration], arXiv:1007.0595 [astro-ph.CO]; *Eur. Phys. J.* **C67** (2010) 39 (arXiv:1002.1028 [astro-ph.GA]).
- [3] C. E. Aalseth *et al.* [CoGeNT Collaboration], arXiv:1002.4703 [astro-ph.CO].
- [4] D. Hooper and L. Goodenough, arXiv:1010.2752 [hep-ph].
- [5] S. Andreas, T. Hambye and M. H. G. Tytgat, *JCAP* **0810**, 034 (2008) (arXiv:0808.0255 [hep-ph]); S. Chang, J. Liu, A. Pierce, N. Weiner, I. Yavin, *JCAP* **1008** (2010) 018 (arXiv:1004.0697 [hep-ph]); R. Essig, J. Kaplan, P. Schuster and N. Toro, arXiv:1004.0691 [hep-ph]; S. Andreas, C. Arina, T. Hambye, Fu-Sin Ling, M. H. G. Tytgat, arXiv:1003.2595 [hep-ph]; D. Hooper, J. I. Collar, J. Hall, D. McKinsey and C. Kelso, *Phys. Rev.* **D88** (2010) 123509 (arXiv:1007.1005 [hep-ph].); R. Foot, *Phys. Lett. B* **692**, 65 (2010) (arXiv:1004.1424 [hep-ph]); A. L. Fitzpatrick, D. Hooper and K. M. Zurek, *Phys. Rev.* **D81** (2010) 115005 (arXiv:1003.0014 [hep-ph]).
- [6] R. Davé, D. N. Spergel, P. J. Steinhardt and B. D. Wandelt, *Astrophys. J.* **547** (2001) 574 (astro-ph/0006218).
- [7] J. McDonald, *Phys. Rev. Lett.* **88** (2002) 091304 (hep-ph/0106249).
- [8] E. Aprile *et al.* [XENON100 Collaboration], *Phys. Rev. Lett.* **105** (2010) 131302 (arXiv:1005.0380 [astro-ph.CO]); arXiv:1005.2615 [astro-ph.CO].

- [9] J. I. Collar and D. N. McKinsey, [arXiv:1005.0838 \[astro-ph.CO\]](#).
- [10] D. S. Akerib *et al.* [CDMS Collaboration], [arXiv:1010.4290 \[astro-ph.CO\]](#). ; Z. Ahmed *et al.* [CDMS Collaboration], [arXiv:1011.2482 \[astro-ph\]](#).
- [11] E. M. Drobyshevski, [arXiv:0706.3095 \[astro-ph\]](#); R. Bernabei *et al.*, *Eur. Phys. J.* **C53**, 205 (2008); N. Bozorgnia, G. B. Gelmini and P. Gondolo, *JCAP* **1011** (2010) 019 ([arXiv:1006.3110 \[astro-ph.CO\]](#)); N. Bozorgnia, G. B. Gelmini and P. Gondolo, *JCAP* **1011** (2010) 028 ([arXiv:1008.3676 \[astro-ph.CO\]](#)).
- [12] M. Fairbairn and T. Schwetz, *JCAP* **0901**, 037 (2009) ([arXiv:0808.0704 \[hep-ph\]](#)).
- [13] C. Kelso and D. Hooper, [arXiv:1011.3076 \[hep-ph\]](#).
- [14] W. Seidel, WONDER 2010 Workshop, Laboratory Nazionali del Gran Sasso, Italy, March 22-23, 2010 ; IDM 2010 Workshop, Montpellier, France, July 26-30, 2010.
- [15] J. Ellis, J. S. Hagelin, D. V. Nanopoulos, K. A. Olive and M. Srednicki, *Nucl. Phys.* **B238** (1984) 453.
- [16] G. Jungman, M. Kamionkowski and K. Griest, *Phys. Rept.* **267** (1996) 195 ([arXiv:hep-ph/9506380](#)).
- [17] E. Kuflik, A. Pierce and K. M. Zurek, *Phys. Rev.* **D81** (2010) 111701; D. Feldman, Z. Liu and P. Nath, *Phys. Rev.* **D81** (2010) 117701 ([arXiv:1003.0437 \[hep-ph\]](#)).
- [18] A. Bottino, N. Fornengo and S. Scopel, *Phys. Rev.* **D67** (2003) 063519 ([arXiv:hep-ph/0212379](#)); A. Bottino, F. Donato, N. Fornengo and S. Scopel, *Phys. Rev.* **D78** (2008) 083520 ([arXiv:0806.4099 \[hep-ph\]](#)); V. Niro, A. Bottino, N. Fornengo and S. Scopel, *Phys. Rev.* **D80** (2009) 095019 ([arXiv:0909.2348 \[hep-ph\]](#)); A. Bottino, F. Donato, N. Fornengo and S. Scopel, *Phys. Rev.* **D72** (2005) 083521 ([arXiv:hep-ph/0508270](#)).
- [19] D. Hooper and T. Plehn, *Phys. Lett.* **B562** (2003) 18 ([arXiv:hep-ph/0212226](#)).
- [20] V. Silveira and A. Zee, *Phys. Lett.* **B161** (1985) 136.
- [21] J. McDonald, *Phys. Rev.* **D50** (1994) 3637.
- [22] C. P. Burgess, M. Pospelov and T. ter Veldhuis, *Nucl. Phys.* **B619** (2001) 709.
- [23] V. Barger, P. Langacker, M. McCaskey, M. J. Ramsey-Musolf and G. Shaughnessy, *Phys. Rev.* **D77** (2008) 035005 ([arXiv:0706.4311 \[hep-ph\]](#)).
- [24] M. Gonderinger, Y. Li, H. Patel and M. J. Ramsey-Musolf, *JHEP* **053** (2010) 1001, 2010 ([arXiv:0910.3167 \[hep-ph\]](#)).
- [25] X.G. He, T. Li, X.Q. Li, J. Tandean and H.C. Tsai, *Phys. Rev.* **D79** (2009) 023521 ([arXiv:0811.0658 \[hep-ph\]](#)).
- [26] J. Angle *et al.* [XENON Collaboration], *Phys. Rev. Lett.* **100** (2008) 021303 ([arXiv:0706.0039 \[astro-ph\]](#)).
- [27] Z. Ahmed *et al.* [CDMS Collaboration], *Phys. Rev. Lett.* **102** (2009) 011301 ([arXiv:0802.3530 \[astro-ph\]](#)); Z. Ahmed *et al.* [CDMS Collaboration], *Science* **327** (2010) 1619 ([arXiv:0912.3592 \[astro-ph.CO\]](#)).
- [28] R. W. Schnee *et al.* [The SuperCDMS Collaboration], [arXiv:astro-ph/0502435](#).
- [29] E. Aprile [Xenon Collaboration], *J. Phys. Conf. Ser.* **203** (2010) 012005.

- [30] K. Nakamura *et al.* [Particle Data Group], J. Phys. **G37** (2010) 075021.
- [31] The effect of η_0 in the one-real-scalar extension of the Standard Model is discussed in D.N. Spergel and P. J. Steinhardt, Phys. Rev. Lett. **84** (2000) 3760 ([astro-ph/9909386](#)). See also [7].
- [32] E. W. Kolb and M. S. Turner, The Early Universe, Addison-Wesley, (1998).
- [33] E. Komatsu *et al.*, [arXiv:1001.4538](#) [[astro-ph.CO](#)].
- [34] S. Weinberg, “Cosmology”, Oxford University Press, (2008).
- [35] A. Abada and S. Nasri, work in progress.
- [36] R. Gaitskell, V. Mandic, and J. Filippini, SUSY Dark Matter/Interactive Direct Detection Limit Plotter, <http://dmtools.berkeley.edu/limitplots>.